



# Liquefaction Mitigation of Silty Sands Using Rammed Aggregate Piers Based on Blast-Induced Liquefaction Testing

Kyle M. Rollins, M.ASCE<sup>1</sup>; Sara Amoroso<sup>2</sup>; Paul Andersen, M.ASCE<sup>3</sup>; Laura Tonni<sup>4</sup>; and Kord Wissmann, M.ASCE<sup>5</sup>

**Abstract:** To investigate the liquefaction mitigation capability of rammed aggregate piers (RAP) in silty sand, blast liquefaction testing was performed at a soil profile treated with a full-scale RAP group relative to an untreated soil profile. The RAP group consisted of 16 piers in a 4 × 4 arrangement at 2 m center-to-center spacing extending to a depth of 9.5 m. Blasting around the untreated area induced liquefaction ( $r_u \approx 1.0$ ) from a 3 to 11 m depth, producing several large sand boils and causing a settlement of 10 cm. In contrast, the installation of the RAP group reduced excess pore water pressure ( $r_u \approx 0.75$ ), eliminated sand ejecta, and reduced the average settlement to between 2 and 5 cm when subjected to the same blast charges. Although the liquefaction-induced settlement in the untreated area could be accurately estimated using an integrated cone penetration test (CPT)-based settlement approach, settlement in the RAP treated area was significantly overestimated with the same approach, even after considering RAP treatment-induced densification. Analyses indicate that settlement after RAP treatment could be successfully estimated from liquefaction-induced compression of the sand and RAP acting as a composite material. This test program identifies a mechanism that explains how the settlement was reduced for the RAP group despite the elevated  $r_u$  values in the silty sands that are often difficult to improve with vibratory methods. DOI: 10.1061/(ASCE)GT.1943-5606.0002563. © 2021 American Society of Civil Engineers.

**Author keywords:** Rammed aggregate piers; Silty sand; Liquefaction; Liquefaction mitigation; Liquefaction-induced settlement; Blast-induced liquefaction; Dense granular columns.

## Introduction

The amount of potential liquefaction-induced settlement in cohesionless soils is related to the initial state criteria of the soil. Looser soils have a higher void ratio and a greater potential to contract under loading than more compact soils. During contraction, the void ratio is reduced, causing settlement associated with volumetric strain. Many ground improvement techniques focus on the densification of the soil, which reduces the void ratio and reduces the potential liquefaction-induced settlement. These techniques include vibrocompaction, rammed aggregate piers (RAP), stone columns, drilled displacement

piles, driven displacement piles, deep dynamic compaction, and blast-densification (Mitchell 1981; Han 2015). Vibratory compaction methods are common forms of densification for cohesionless soils, as both loose and medium-dense sands will experience densification during vibration (Castro 1969). Extensive research has shown that vibrational ground improvement techniques are effective in densifying sands with less than about 15% fines (D'Appolonia 1954; Mitchell 1981; Baez 1995; Adalier and Elgamil 2004; Wissmann et al. 2015; Vautherin et al. 2017).

In contrast, vibratory compaction techniques become progressively less effective in silty sands as the fines content and plasticity increase (Saito 1977; Mitchell 1981; Leurhing et al. 2001). Increasing fines content strengthens the soil structure and decreases the permeability, preventing pore pressure dissipation so that there is less densification. In these conditions, it may be necessary to increase the area replacement ratio (area of the column/tributary area) to 20%–25% and/or use prefabricated drains between columns to achieve significant improvement (Allen et al. 1995; Leurhing et al. 2001; Rollins et al. 2009). As the fines content increases, other ground improvement techniques, such as vibratory replacement or soil mixing, are often preferred. Examples of such types of ground improvement are summarized by Han (2015). Vibratory replacement improves less compactible materials by the installation of load-bearing columns of well-compacted, coarse-grained backfill material (Priebe 1995). These techniques mitigate against liquefaction by increasing soil density, increasing the mean stress, providing drainage for excess pore water pressures, and increasing the stiffness and shear resistance of the soil (Priebe 1998). Soil mixing creates a grid of soilcrete panels that provide increased lateral resistance and reduce the potential for liquefaction of sand within each grid (Namikawa et al. 2007).

Current cone penetration test (CPT)- and standard penetration test (SPT)-based liquefaction-induced settlement evaluation techniques

<sup>1</sup>Professor, Dept. of Civil and Environmental Engineering, Brigham Young Univ., 430 Engineering Building, Provo, UT 84602 (corresponding author). ORCID: <https://orcid.org/0000-0002-8977-6619>. Email: rollinsk@byu.edu

<sup>2</sup>Assistant Professor, Dept. of Engineering and Geology, Univ. of Chieti-Pescara, Viale Pindaro 42, Pescara 65129, Italy; Research Associate, Istituto Nazionale di Geofisica e Vulcanologia, Viale Francesco Crispi 43, L'Aquila 67100, Italy. ORCID: <https://orcid.org/0000-0001-5835-079X>. Email: sara.amoroso@unich.it

<sup>3</sup>Research Assistant, Dept. of Civil and Environmental Engineering, Brigham Young Univ., 430 Engineering Building, Provo, UT 84602. Email: paul.andersen@byu.edu

<sup>4</sup>Associate Professor, Dept. of Civil, Chemical, Environmental, and Materials Engineering, Univ. of Bologna, Viale del Risorgimento 2, Bologna 40136, Italy. Email: laura.tonni@unibo.it

<sup>5</sup>President and Chief Engineer, Geopier Foundation Co., 130 Harbour Place Dr., Suite 280, Davidson, NC 28036. Email: KWissmann@geopier.com

Note. This manuscript was submitted on April 27, 2020; approved on March 18, 2021; published online on June 25, 2021. Discussion period open until November 25, 2021; separate discussions must be submitted for individual papers. This paper is part of the *Journal of Geotechnical and Geoenvironmental Engineering*, © ASCE, ISSN 1090-0241.

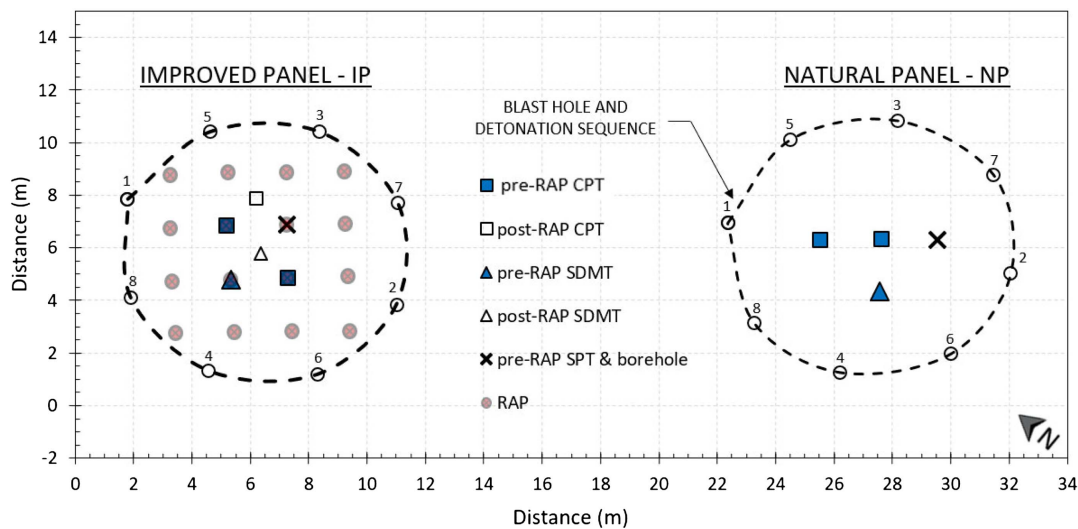


Fig. 1. Locations of in situ tests and blast holes in the natural panel (NP) and improved panel (IP).

typically account for increased density produced by various ground improvement methods and generally do not comprehensively consider other improvement mechanisms (e.g., Youd et al. 2001; Zhang et al. 2002). For RAPs, these mechanisms include a composite response (Lawton and Fox 1994; Demir et al. 2017), increased lateral pressure (Harada et al. 2010), and increased shear stiffness (Green et al. 2008), which has been the subject of numerous recent studies for both RAPs and stone columns (Pestana and Goughnour 1998; Green et al. 2008; Olgun 2003; Rayamajhi et al. 2015). Furthermore, there are only a limited number of published studies demonstrating RAP effectiveness in mitigating liquefaction in sandy silts and silty sands (Amoroso et al. 2018; Wissmann et al. 2015; Saftner et al. 2016; Smith and Wissmann 2018).

To understand better the potential for liquefaction mitigation and settlement reduction in sand with high fines content using RAP treatment, two full-scale blast tests were performed at a silty sand site in Bondeno, Italy (near Ferrara) in which liquefaction was observed after the 2012  $M_W$  6.1 Emilia Romagna earthquake (Emergeo Working Group 2013), as preliminarily presented by Amoroso et al. (2019). Blast testing has been performed previously to evaluate the lateral resistance of piles (Rollins et al. 2005), the improvement from stone column treatment (Ashford et al. 2000; Weaver et al. 2004), the improvement from colloidal silica grouting (Gallagher et al. 2007), the improvement from driven displacement piles (Gianella and Stuedlein 2017), earthquake drain effectiveness (Rollins et al. 2004) and also to compare a variety of ground improvement techniques in Christchurch, New Zealand (Wentz et al. 2015). In Bondeno, one blast test was performed around a profile treated with a group of 16 RAPs and referred to as the improved panel (IP), while another blast test was performed on an adjacent untreated natural panel (NP) to provide a control section for comparison. This paper compares the performance of the natural and improved panels in terms of excess pore pressure and settlement and then evaluates various models for computing settlement in comparison with measured profiles.

### Site Location and Characterization

The location of the Bondeno test site was selected based on surface evidence of liquefaction that was noted during the 2012 earthquake sequence in the region. Geotechnical in situ tests were performed at a few potential sites around Bondeno until a suitable site was identified with a relatively uniform layer of liquefiable

silty sand. A plan view drawing showing the locations of the natural and improved panels, defined by rings of blast holes, is provided in Fig. 1.

Results from the in situ piezo cone penetrometer test (CPTu) and dilatometer (DMT) testing at the natural panel (NP) and improved panel (IP) before RAP installation (pretreatment) are shown in Fig. 2. The CPTu sounding at both profiles was continued to a 15-m depth. The DMT investigation in the IP was discontinued at an 11.5 m depth due to technical difficulty advancing the dilatometer blade. As seen in Fig. 2, the profile consists of a surface layer composed of silty clay and clay (CL) to a depth of 3.5 m, underlain by silty sand (SM) to a depth of 12.6 m, which is, in turn, underlain by sands and silty sands (SP-SM). Geological investigations found that the silty sand layers from 3.5 to 12.6 m consist of Holocene alluvial deposits in a paleochannel of the Po River, while the deeper sand and silty sand layers are late Pleistocene glacial braided Po river deposits (Regione Emilia-Romagna 1998; Amoroso et al. 2020). The cohesive soil layer has an average plasticity index ( $PI$ ) of 20% and a soil behavior type index ( $I_c$ ) greater than 2.6; therefore, liquefaction and liquefaction-induced settlement would not be expected from 0 to 3.5 m below ground (Robertson and Wride 1998; Boulanger and Idriss 2016; Bray and Sancio 2006).

The corrected cone tip resistance ( $q_t$ ) and the soil behavior type index ( $I_c$ ) values from the CPTu are very similar for the NP and IP sites, as are the fines contents estimated using a correlation proposed by Robertson and Wride (1998). However, measured fines contents in the sand layers are typically between 20% and 40% and are considerably higher than those interpreted from the correlation. This is consistent with results based on a 2,600-point data set in Christchurch, New Zealand (Maurer et al. 2015), where significant scatter from predicted fines content was observed. In this study, the clean sand equivalent has been determined using the  $I_c$  value, which is a function of both fines content and plasticity, as suggested by Robertson and Wride (1998).

The profiles of the earth pressure coefficient ( $K_0$ ), obtained from the DMT testing using the Marchetti (1980) formula in the cohesive layer and from the combined CPT-DMT data in the sandy deposits according to Baldi et al. (1986), and of the shear wave velocity ( $V_s$ ), measured by the seismic dilatometer test (SDMT) according to Marchetti et al. (2008), also show reasonably good agreement between the two panels, particularly in the sand layers.

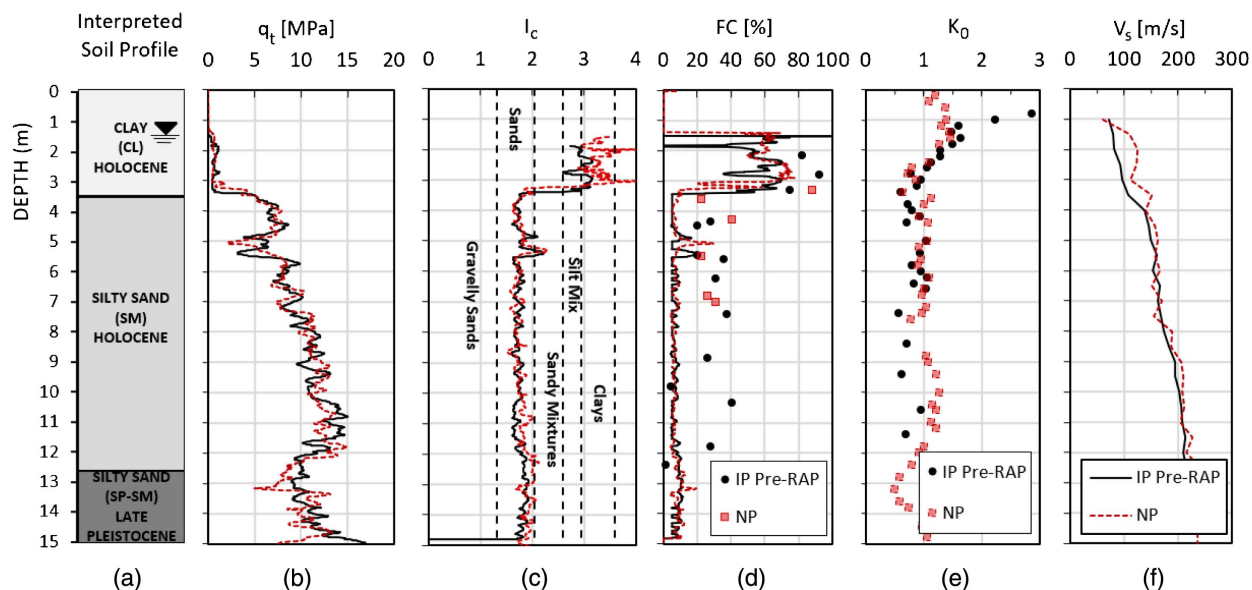


**Fig. 2.** (a) Interpreted soil profile and comparisons of CPTu and SDMT test results at the natural panel (NP) and the pre-RAP treatment improved panel (IP) with respect to (b) corrected cone tip resistance,  $q_t$ ; (c) soil behavior type,  $I_c$ ; (d) fines content,  $FC$  from the Robertson and Wride (1998) correlation and disturbed SPT samples; (e) at-rest earth pressure coefficient,  $K_0$ ; and (f) shear wave velocity,  $V_s$ .

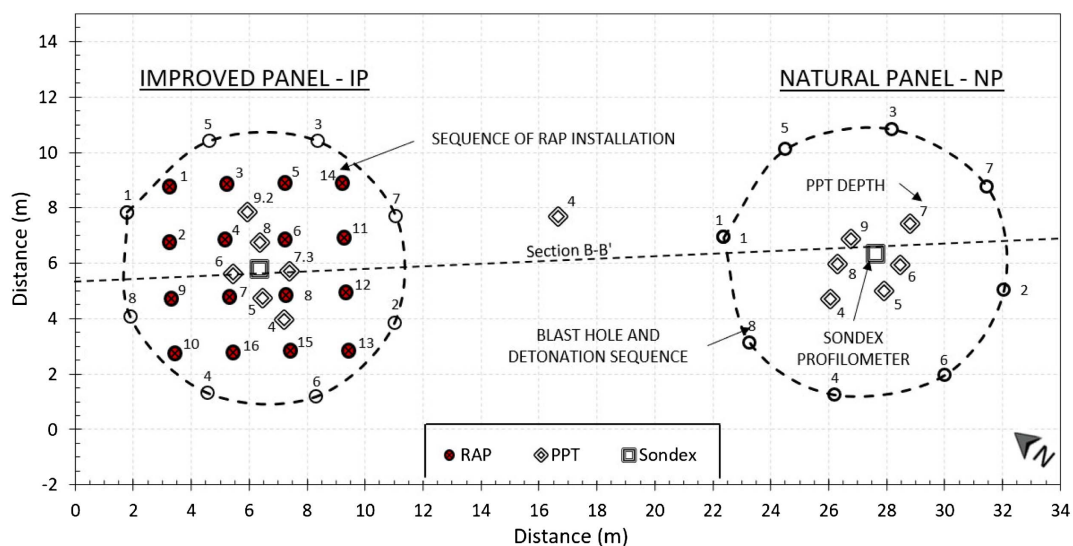


**Fig. 3.** Locations of blast holes, RAP columns, pore pressure transducers (PPTs), and profilometers for the natural and improved panels. Numbers by blast holes indicate detonation sequence, numbers by RAP columns indicate construction sequence, numbers by PPTs indicate depth.

### RAP Group Layout and RAP Installation

Over a 3-day period, the 0.5 m diameter RAP columns were installed to a target depth of 9.5 m in a  $4 \times 4$  quadrangular grid covering a  $6.5 \times 6.5$  m area, with a 2-m center-to-center spacing, as shown in Fig. 3.

The RAP elements were constructed by a RAP-licensed affiliate using displacement techniques with an excavator-mounted mobile ram base machine fitted with a high frequency (30–40 Hz) vibratory hammer, as illustrated in Fig. 4. The base machine drives a 250–300 mm outside diameter open-ended pipe mandrel fitted with a specially designed 350–400 mm diameter tamper foot into the ground. A sacrificial cap or internal compaction mechanism prevents soil from entering the tamper foot and mandrel during

driving. After driving to the designed depth, the hollow mandrel serves as a conduit for aggregate placement. Placed inside, the aggregate flows to the bottom of the mandrel. The tamper foot and mandrel are then raised approximately 0.9 m and then driven back down 0.6 m, forming a 0.3-m thick compacted lift. Compaction is achieved through static downforce and dynamic vertical ramming from the hammer. The process densifies aggregate vertically, and the beveled tamper foot forces aggregate laterally into the cavity sidewalls. This process typically required about 45 min of compaction for every 9.5-m long pier. The construction methods have been shown to increase the density of the pier aggregate to greater than  $22 \text{ kN/m}^3$  (Lawton and Merry 2000), providing a friction angle greater than  $45^\circ$  (White et al. 2002).

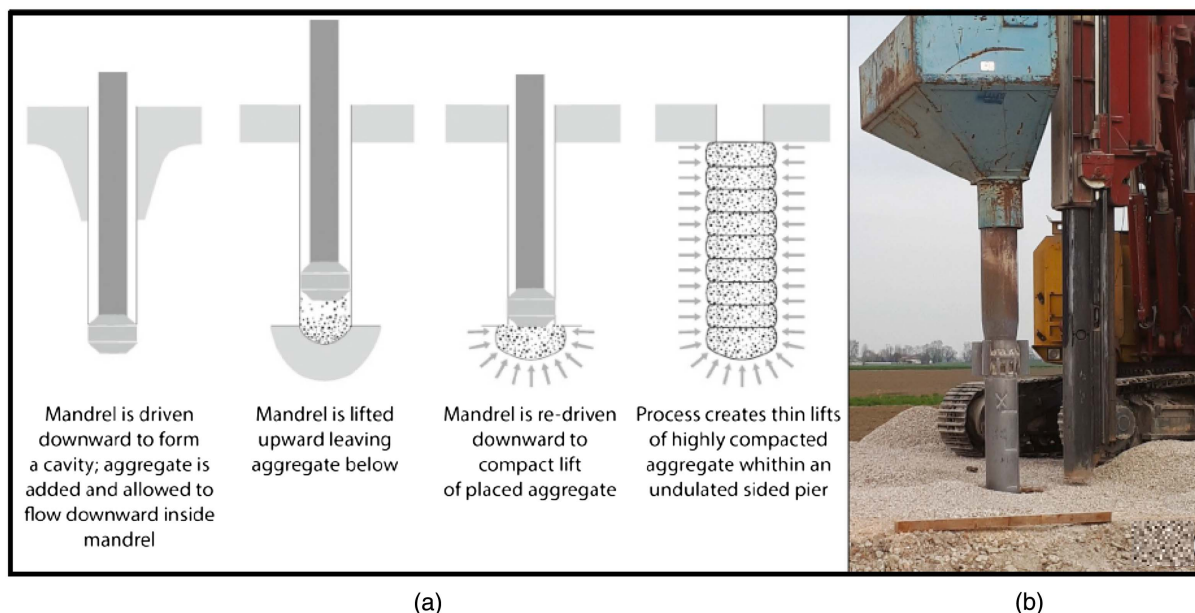


**Fig. 4.** (a) Simplified representation of RAP construction process; and (b) photograph of RAP installation at the Bondeno test site. [Reprinted from *Engineering Geology*, 265, S. Amoroso et al., "Blast-induced liquefaction in silty sands for full-scale testing of ground improvement methods: Insights from a multidisciplinary study," 105437, © 2020, with permission from Elsevier.]

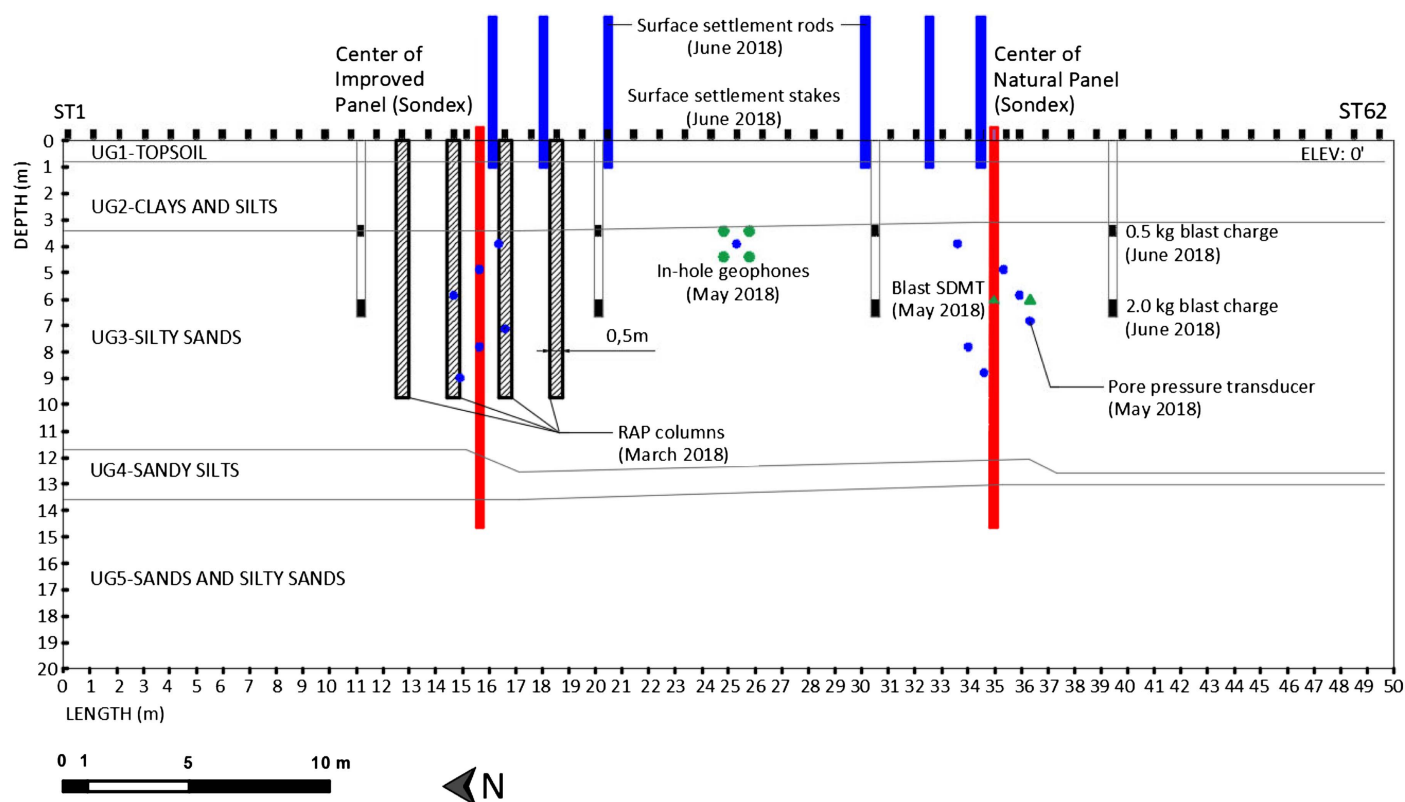


**Fig. 5.** Simplified soil profile through section B-B' (see Fig. 3) showing the relative positions of the improved panel (IP) and the natural panel (NP), RAP column positioning, blast holes, and other instrumentation at the site.

Crushed aggregate was fed through the mandrel from a top-mounted hopper and compacted in the displaced cavities to create a 0.5 m diameter, dense, stiff aggregate pier element. The aggregate consisted of crushed limestone with an angular particle shape and a  $D_{50}$  size of 12.5 mm. The aggregate had a very uniform gradation with a coefficient of uniformity ( $C_u$ ) of 1.27 and a

coefficient of gradation ( $C_c$ ) of 0.94. The construction methodology has been described in more detail by Majchrzak et al. (2009) and Saftner et al. (2018).

The RAP installation process was intended to densify and increase the lateral earth pressure in the surrounding soil while constructing a dense aggregate column. The 2-m on-center installation

pattern is the same as that successfully implemented for a previous test site in similar soil conditions (Wissmann et al. 2014). The installation pattern produced an area replacement ratio ( $R_a$ ), defined as the ratio of the pier area to the 2-m square tributary soil area surrounding the pier, equal to 5%. Based on experience, this area ratio was expected to increase the cone tip resistance by 1–4 MPa (20%–30%), depending on the fines content and initial tip resistance. This was intended to increase the factor of safety against liquefaction ( $FS_L$ ) above 1.25 based on Eurocode 8 (CEN 2004) for the design earthquake ( $M_W = 6.14$ ,  $a_{max} = 0.22$ ) or reduce settlement to less than about 2.5 cm. Nevertheless, predicting improvement in silty sand is difficult, and the experiment provides an opportunity to measure actual improvement based on a variety of in situ tests.

Ten RAPs were evaluated using an index test known as a crowd stabilization test (CST) at three depths in each pier during installation (Geopier Foundation Company 2019). In these tests, a downward pressure of 14 MPa was applied to the pier by the installation machine, and the settlement was measured. The average settlement for the first three piers was 123 mm, while the average for the remaining piers decreased to 18 mm. A settlement less than 25–50 mm is typical of a well-compacted pier. Clearly, the first three piers were not as well compacted while the stroke pattern and mandrel lifting rate were being refined for the project. Two pilot piers would normally be used to make these adjustments for a commercial project. Flow rate tests were also performed to confirm the measurement of the inserted volume. The order of installation of the pier numbers is shown in Fig. 3. Fig. 5 provides a simplified cross-section after RAP installation along Section B-B' in Fig. 3.

## Post-RAP Ground Improvement Evaluation

Additional geotechnical in situ tests (CPTu and SDMT) were conducted at the center points between RAPs, as shown in Fig. 3, after the installation of the RAP columns to quantify the improvement. Fig. 6 provides plots of the corrected cone tip resistance  $q_t$ , soil behavior type index  $I_c$ , relative density  $D_r$ , in situ earth pressure coefficient  $K_0$ , and  $FS_L$ . The preimprovement plots are from one seismic dilatometer performed to an 11.4-m depth, the post

improvement characteristics are plotted from one seismic dilatometer performed between a 0 and 4.8-m depth, and one Medusa dilatometer performed between a 4.6- and 11.2-m depth. The Medusa dilatometer is a new DMT device that combines the flat dilatometer with hydraulic automation and a measuring system for autonomously performing DMT tests (Marchetti et al. 2019). As anticipated, no improvement occurred from the RAP installment in the clay layer between a 0 and 3-m depth. Between the depths of 4 and 9 m, the corrected cone tip resistance ( $q_t$ ) and horizontal stress index ( $K_D$ ) each experienced significant improvement 1 month after RAP installation, about 30% and 50%, respectively. The relative density computed using a correlation with CPT cone resistance (Jamiolkowski et al. 2003) also shows a moderate improvement (approximately 13%) within the layer of interest. The increase in  $K_D$  suggests a significant increase in lateral earth pressure due to the RAP treatment. In sandy layers,  $K_0$  can be estimated by coupling data from CPT and DMT data, according to Baldi et al. (1986). Post-RAP  $K_0$  values increased about 30% between a 4- and 7-m depth and 100% between a 7- and 9-m depth in comparison to the natural soil conditions.

The  $FS_L$  was computed using the well-established CPTu-based procedure proposed by Idriss and Boulanger (2008). The liquefaction susceptibility analyses were performed for a moment magnitude  $M_W = 6.14$  (Meletti et al. 2008) and a peak ground acceleration,  $a_{max} = 0.22$  g (Stuchi et al. 2011). For this analysis, the water table was assumed to be at 0.5 m during the earthquake event. These values correspond to those used in ongoing seismic microzonation studies of the Bondeno municipality for a return period of 475 years. Prior to treatment, liquefaction would be predicted between 3.5 and 8 m with an average  $FS_L$  of 0.87. After treatment, the  $FS_L$  profile shows a significant increase with an average  $FS_L$  of 1.28 between 3.5 and 8 m. The  $FS_L$  increases most significantly in the zone between 5.5 and 8.0 m, where the average  $I_c$  is 1.71, relative to the zone from 3.5 to 5.5 m where the average  $I_c$  is 1.82 and  $I_c$  exceeded 2.0 in two layers. Similar sensitivity of ground improvement to  $I_c$  variation has been observed for stone column treatment in silty sands (Rollins et al. 2012).

Some context for the improvement produced by the RAP treatment can be provided by referencing improvement from other

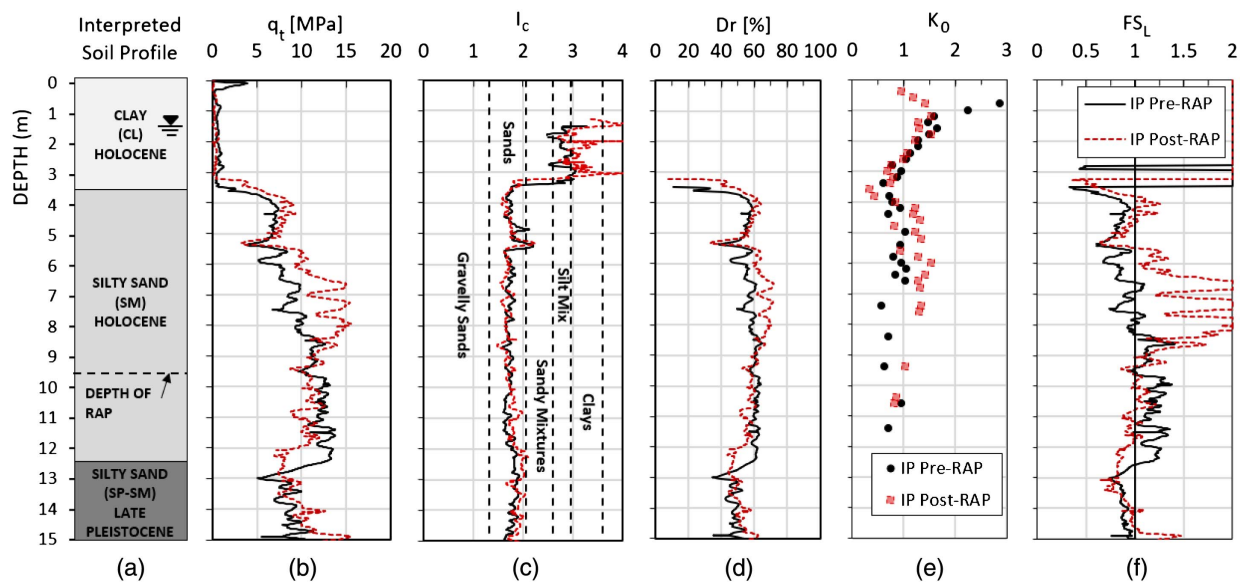


**Fig. 6.** Effects of RAP improvement within (a) the interpreted soil profile, as measured by the (b) CPT cone tip resistance,  $q_t$ ; (c) soil behavior type index,  $I_c$ ; (d) relative density,  $D_r$ ; (e) at-rest earth pressure coefficient,  $K_0$ ; and (f) factor of safety against liquefaction,  $FS_L$ .

ground improvement strategies in sands with similar high fines contents. Rollins et al. (2009) report that stone column treatment at a freeway overpass in Utah was able to produce average increases of 79% and 33% in the SPT penetration resistance in silty sands with an average fines content of 30% and 40%, respectively. However, this improvement required an area replacement ratio of 26% in comparison with the 5% replacement ratio for the RAP group in this study. Similarly, Allen et al. (1995) report that stone column treatment at Mormon Island Dam in California increased the average SPT ( $N_1$ )<sub>60</sub> from about 12 to 27 (125%) in a 6-m thick layer of silty sand with 30% average fines content. But this improvement also required a replacement ratio of 26%.

## Blasting Process and Instrumentation Layout

A total of 16 explosive charges were detonated during each blast test. The charges were placed around the periphery of two 10-m diameter circles, as shown in Fig. 3. Eight blast holes were cased to a depth of 7 m at 45° intervals around the perimeter of the rings. Explosive charges (dynamite with a detonation velocity of 5,900 m/s) were installed at two different levels within the liquefiable layer: 0.5 kg at 3.5 m and 2.0 kg at 6.5 m with gravel stemming between them to increase blast pressure in the horizontal direction. The explosive charges were detonated sequentially at 1 s intervals with the detonation of the bottom charge followed by the upper charge in each blast hole. The sequence of blasting is indicated adjacent to the blast hole in Fig. 3, with blast holes alternating from opposite sides of the ring. The blasts of the two panels were conducted separately (i.e., Blast 1 for the NP and Blast 2 for the IP) to limit the effects of superposition and simplify the comparison of the effects of the blast-induced liquefaction on the IP and the NP separately. At the center of each panel, a Sondex profilometer (with a resolution of 0.3 cm) was installed to a depth of 15 m to record the settlement versus depth in the profile.

Pore pressure transducers (PPTs) were installed at depths of 4, 5, 6, 7, 8, and 9 m in each test panel at a distance of 1–2 m from the panel center (Fig. 3) to measure the generation and subsequent dissipation of the excess pore pressures induced by the blast. The PPTs had a resolution to 0.7 kPa with a 3,450 kPa maximum range and an overpressure limit of five times. Six survey poles were placed within the NP (P1, P2, and P3) and the IP (P4, P5, and P6) to monitor ground surface settlement with time after the blast. Conventional survey measurements were made using a Topcon DI-502 digital auto level, which measured ground surface settlements to 0.03 cm (0.001 ft) accuracy along a linear array of 62 survey stakes (ST) following each blast. Finally, terrestrial laser scanning (TLS) and structure from motion (SfM) aerial photogrammetry were used to create point clouds and digital terrain models (DTMs) that provided the overall pattern of the ground surface settlement for each test blast.

Explosives were installed on the day of the blast for safety reasons. The first blast took place in the NP at 12:22:35 local time, followed by the second blast in the IP several hours later at 15:24:56 in order to study the effect of the blast-induced liquefaction on the NP and IP separately. The excess pore pressure ratio,  $r_u$ , returned to static levels approximately 6 and 5 min after the first and second blast sequences, respectively.

## Results from Blast 1 Around Natural Panel and Blast 2 Around Improved Panel

The pore pressure response and resulting settlement in the NP and the IP from the two identical blast events are compared in the subsequent sections.

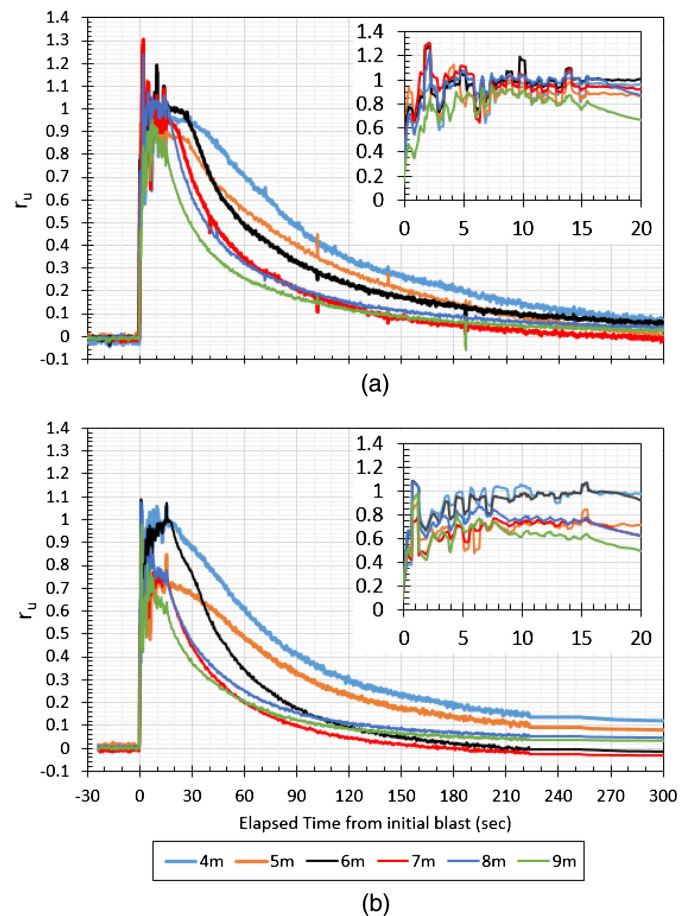


**Fig. 7.** Excess pore pressure ratio versus time recorded following (a) Blast 1 in the NP; and (b) Blast 2 in the IP at 4, 5, 6, 7, 8, and 9 m depths. The excess pore pressure ratio versus time during the blast is shown in the inset.

## Excess Pore Pressure Measurements

The excess pore pressure ratio ( $r_u$ ), defined as the excess pore pressure ( $\Delta u$ ) divided by the initial vertical effective stress ( $\sigma'_{vo}$ ), was monitored during and after each blast sequence. Pore pressure transducer (PPT) measurements made at a sampling rate of 100 Hz were smoothed with a 100-point moving average to remove the majority of the transient pulses and better represent the residual pore pressure. Plots of the residual excess pore pressure ratio versus time are provided in Figs. 7(a and b) for the six transducers in the NP and IP, respectively. The inset plots in Figs. 7(a and b) show each data point within the blast window and includes transient spikes during the blast sequence.

For each charge detonation, a transient pressure spike developed, followed by an increase in the residual excess pore pressure ratio. At both panels, excess pore pressures rapidly developed after a few seconds and remained at their peak for 15–20 s before dissipating. The  $r_u$  values dissipated from the bottom upwards and decreased to essentially static levels within about 6 min after blast detonation. In the improved panel, the blasting sequence generated somewhat lower peak  $r_u$  values, and the dissipation rate was somewhat more rapid in comparison with the natural panel.

The peak residual  $r_u$  values for the IP and NP are plotted versus depth in Fig. 8. In the NP during Blast 1, the peak measured  $r_u$  values are close to 1.0 from 3 to 9 m, indicating liquefaction. In contrast, the peak  $r_u$  values in the IP during Blast 2 are generally

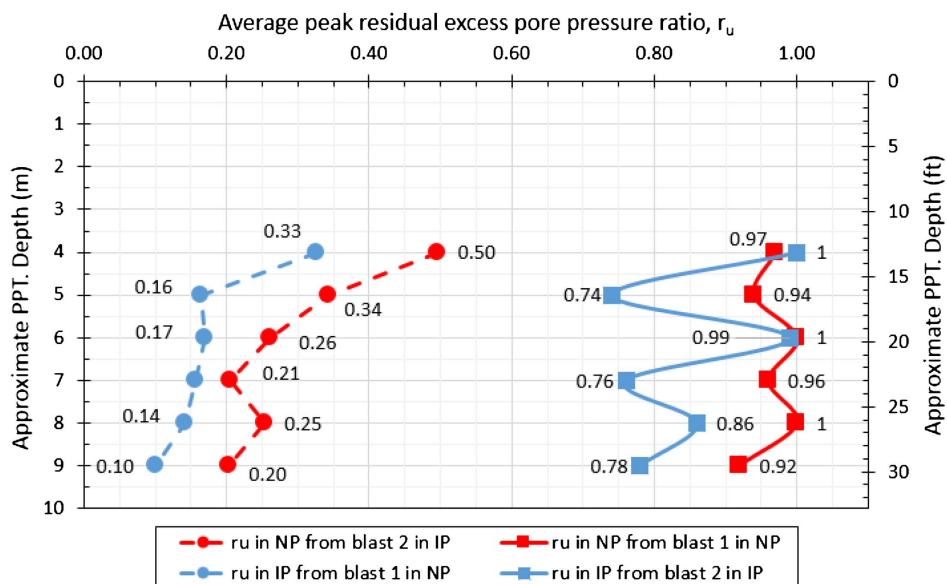


**Fig. 8.** Comparison of peak excess pore pressure ratio,  $r_u$ , measured during Blast 1 in the natural panel (NP) and Blast 2 in the improved panel (IP).

lower than 1.0, indicating that the RAP columns were effective in reducing the generation of excess pore pressures. The postimprovement  $D_r$  and  $K_0$  profiles from Fig. 6 suggest that increased density and lateral earth pressures were, in part, responsible for the reduction in potential excess pore pressure generation. Significant  $r_u$  reductions from NP are seen at depths of 5, 7, 8, and 9 m. At these depths, the peak residual  $r_u$  was kept below the 80% limit for incipient liquefaction suggested by Studer and Kok (1980). In both the NP and the IP, larger  $r_u$  values were observed at depths of 4 and 6 m. These higher  $r_u$  values at 4 and 6 m are likely due to the coplanar placement of the blast charges at nearly corresponding depths. In the NP, the average peak  $r_u$  excluding the 4 and 6 m transducers was 95%, compared to 78% in the IP. Fig. 7 shows that for both the NP and the IP, the rate of excess pore pressure dissipation recorded in the 4, 5, and 6 m PPTs was significantly slower than in the PPTs at 7, 8, and 9 m. During the blast sequence on the opposite side of the field, that is, the north side of the field for the blast in the NP and the south side of the field for the blast in the IP, some level of  $r_u$  generation was produced. Fig. 8 shows that the  $r_u$  values were slightly higher in the NP than in the IP, although they were below the level for incipient liquefaction.

### Sand Ejecta

Following blasting, several large sand boils developed within the blast ring in the natural panel, as shown in the photograph in Fig. 9. These characteristic liquefaction features visually confirm the results of the pore pressure measurements. Mineralogical evaluation of the ejecta from the sand boil with sand from SPT testing indicates that the ejecta likely came from liquefaction in the depth interval between 3 and 9 m (Amoroso et al. 2020).

In contrast to the natural panel, no sand boils formed within the area treated with RAP columns, although smaller sand boils developed outside the treated zone. Considering that the development of ejecta was a major cause of building damage during liquefaction in the Christchurch earthquake sequence (van Ballegooy et al. 2014), this appears to be an important benefit of RAP treatment. Ejecta typically emerged at boreholes used to install instrumentation and blast holes; however, the same pathways existed in both the NP and the IP.

### Pore Pressure-Induced Settlements

#### Ground Surface Settlements

Ground surface settlements for Blasts 1 and 2, based on elevation change of the survey stakes, are plotted in Fig. 10. Survey measurements were performed between 30 and 60 min after the blast when excess pore pressure had fully dissipated. Reconsolidation following blast-induced liquefaction produced a nearly symmetrical settlement pattern across the NP, as shown in Fig. 10 for the first blast. The maximum settlement at the center of the blast ring was about 95 mm, and the settlement decreased to zero at a distance of about 12 m from the center of the blast ring. Settlements within the blast ring were between 70 and 95 mm after Blast 1.

The elevation change was also measured using terrestrial laser scanning (TLS) and color contours of settlement after both blasts are provided in Fig. 11. The settlement contours indicate a circular dish-shaped settlement pattern in the natural panel similar to the auto-level measurements; but the TLS settlements are somewhat lower. This is because sand ejecta accumulating at the ground surface decreases the settlement recorded by the TLS relative to that from the



**Fig. 9.** Multiple sand boils and ejecta, the evidence of liquefaction, observed during Blast 1 near the center of the unimproved natural panel (NP). (Image by Kyle M. Rollins.)

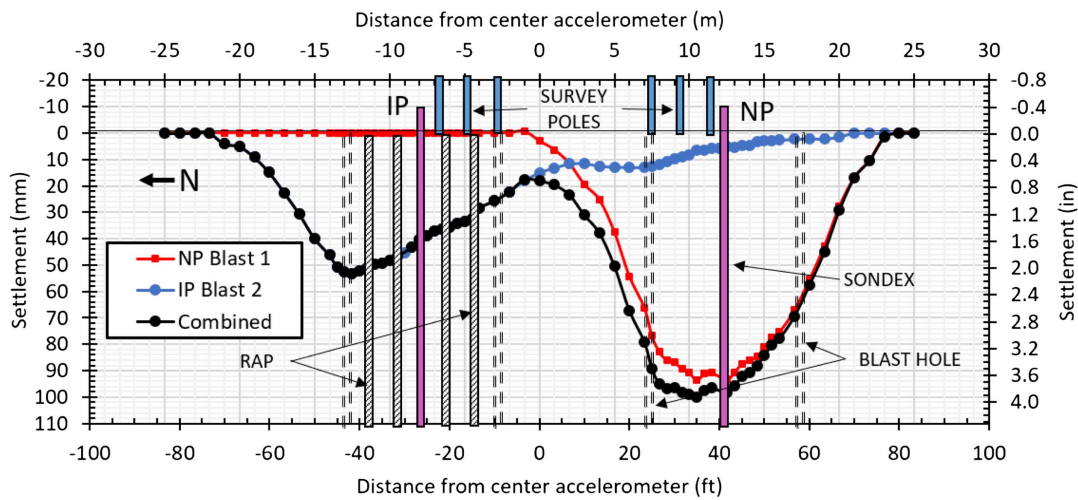


**Fig. 10.** Comparison of ground settlement measurements obtained 30 min after Blast 1 in the NP and Blast 2 in the IP along section B-B' (see Fig. 3). The combined settlement from Blasts 1 and 2 is also plotted.

survey stakes. Additional details about the TLS-based settlement are provided by Amoroso et al. (2020).

The settlement caused by the second blast is also shown in Fig. 10, along with the settlement induced by the first blast. The second blast produced both settlements within the IP and some additional settlement in the NP, which could have been due to strain softening during the first blast sequence. Both the TLS and autolevel surveys confirm that the settlement in the IP was between 20 and 50 mm, which is considerably less than that in the natural panel.

The surface settlement from the second blast sequence did not exhibit a symmetric settlement profile, as was observed in the NP, but was higher on the north side (Fig. 10) and northeast corners of the panel (Fig. 11) relative to the rest of the treated area. One likely explanation for these higher settlements is the lower construction quality during the installation of the first three RAPs, as described previously. The crowd stabilization test results demonstrate that the RAPs on the northeast side of the IP, which were the first to be constructed, settled more during crowd stabilization tests than the other RAPs in the grid. This lower RAP quality led to lower RAP column stiffness and less densification around these columns during treatment.

### Settlement versus Depth Measurements

Settlement versus depth was also measured in both panels by means of a Sondex profilometer, consisting of a corrugated pipe

containing metal rings surrounding an access tube for a measurement probe. As the soil surrounding the corrugated pipe settled during pore pressure dissipation, the corrugated pipe is simultaneously compressed to match the soil settlement. The locations of the metal rings around the corrugated pipe are measured with a probe before and after blasting in order to compute the settlement. The settlement with a depth in the NP as measured by the Sondex profilometer is provided in Fig. 12.

The Sondex settlement provided data consistent with expectations based on soil stratigraphy and the measured ground surface settlement. The clay and organic soil within the top 3 m did not compress but settled along with the underlying sand. Liquefaction-induced settlement occurred within the layers of sandy-silt and silty-sand between a 3- and 11-m depth. Below 11 m, the Sondex measurements in the NP area consistently showed that no settlement occurred, indicating the pore pressure induced settlement was insignificant below 11 m. The average volumetric strain within the liquefied zone was approximately 1.6% from 3 to 8 m and approximately 0.8% from 8 to 11 m.

The settlement profile shown in Fig. 12 illustrates the significant reduction in the settlement in the zone of RAP treatment (3–9.5 m) and a reduction of maximum surface settlement of approximately 6 cm. Of interest, the measurements indicate that less than 2 cm of compression occurred within the region of improvement in comparison to about 8 cm of compression in the natural panel, a 75% settlement reduction. In contrast to the profilometer in the NP, the settlement in the IP did not decrease to zero at a depth of 11 m, although the pore-pressure induced settlement was likely insignificant below this depth as indicated by the natural panel settlement profile. This suggests that an additional mechanism may be responsible for the observed settlement of about 1 cm below this depth. A few inconsistencies exist in the settlement with depth profiles provided in Fig. 12, such as the points at which settlement appears to be less at a shallow depth than at a deeper depth. These inconsistencies may be due to local slippage or irregular compression of the pipe.

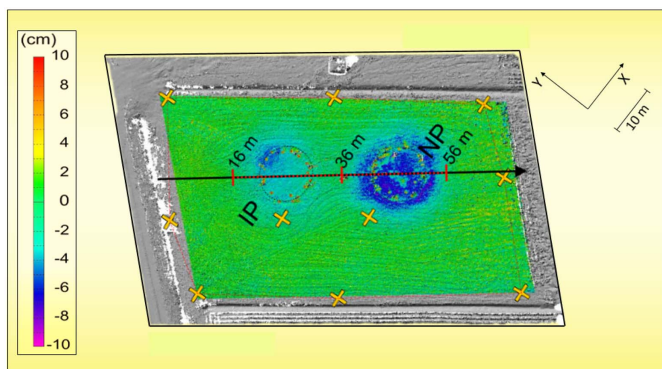


**Fig. 11.** Color contour map of cumulative settlement after the two blast tests from TLS surveys (including data from Amoroso et al. 2020).

### Ground Surface Settlement versus Time

Ground settlement due to liquefaction-induced reconsolidation was measured with time using autolevel readings on three survey poles embedded 0.5 m into the surface clay layer inside the blast ring. The autolevel tripod was positioned approximately 20 m NE

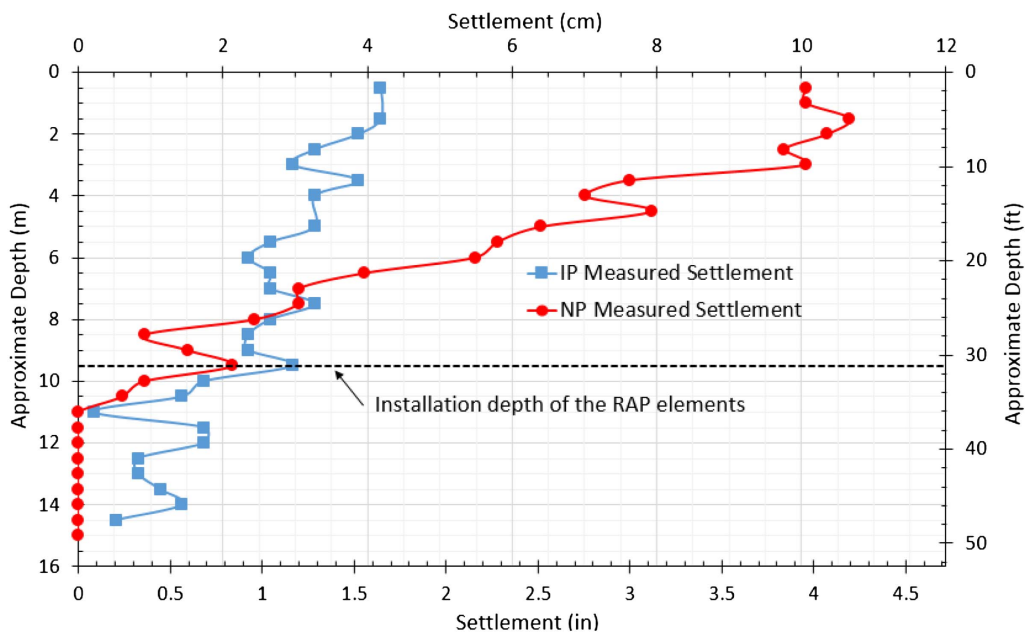


**Fig. 12.** Comparison of observed settlement with the depth in the NP and the IP as measured by the Sondex profilometer after Blasts 1 and 2, respectively.

and 35 m NE from the centers of the IP the NP, respectively, beyond the limit of the ground settlement. The total settlements with time for the NP and IP are plotted in Figs. 13(a and b), respectively. Settlement normalized by the maximum settlement for each pole is plotted in Figs. 13(c and d), respectively. After normalization by the maximum settlement, the three settlement versus time curves generally plot on top of each other. In the NP, between 65% and 80% of the total settlement occurred within the first 2 min when the average  $r_u$  had decreased to 80%. Approximately 95% of the total settlement occurred within 13 min while the average  $r_u$  values were nearly zero at 15 min. The average excess pore pressure ratio between a 4- and 9-m depth dissipated to 60% of its initial value within 25s of the final charge of the blast sequence.

In the improved panel, 95% of the settlement was completed within only 8 min, which is approximately 60% of the time required for a 95% settlement in the NP. The increased rate of settlement is likely a result of horizontal drainage to the RAP columns in the improved panel. However, a lower modulus of compressibility in the silty sand would also have produced less water volume to be dissipated.

Significant reductions in settlement, excess pore pressures, and ejecta were also observed in blast liquefaction tests evaluating driven displacement piles (Gianella and Stuedlein 2017), RAPs in Christchurch, New Zealand (Wissmann et al. 2015), and stone columns at Treasure Island (Ashford et al. 2000) with similar  $R_a$  values. However, the contents of the fines at these sites were between 5% and 10%, whereas the contents of the fines at this site were considerably higher (15%–45%), making ground improvement more difficult.

## Settlement Analysis

### Computed Settlement of the NP based on CPT Resistance

The observed settlement profile in the natural panel indicates that liquefaction-induced settlement occurred between the 3- and 11-m

depths, as evidenced by Fig. 12. Little to no settlement occurred within the 3-m thick cohesive surface layer, which was nonliquefiable, and no settlement occurred below 11 m in the natural panel. Within the liquefied layers from 3 to 11 m, the CPT-based volumetric strain equations proposed by Zhang et al. (2002) were used to compute liquefaction-induced settlement relative to measured settlement in both the natural panel and the improved panel prior to the installation of the RAP columns. Zhang et al. (2002) use the cyclic liquefaction tests and reconsolidation settlement measurements from Ishihara and Yoshimine (1992) to develop volumetric strain equations. The Ishihara and Yoshimine curves are based only on relative density and  $FS_L$ . Zhang et al. (2002) developed a correlation to estimate relative density based on the normalized cone penetration resistance for clean sand ( $q_{c1N}$ )<sub>cs</sub> obtained from  $I_c$ . One can then compute volumetric strain knowing ( $q_{c1N}$ )<sub>cs</sub> and  $FS_L$ .

Although blasting clearly produced liquefaction based on pore pressure ratios and ejecta, the factor of safety against liquefaction, in this case, cannot be obtained using simple liquefaction triggering equations developed for earthquakes. However, the  $FS_L$  can be computed directly from the number of blast charges required to produce liquefaction in the field in comparison with the first eight large blast charges. Each blast charge typically produced one cycle of loading based on downhole ground motion recordings.

Seed and Idriss (1982) developed magnitude scaling factors ( $MSF$ ) to adjust the cyclic resistance ratio ( $CRR$ ) relative to an  $M_w 7.5$  earthquake producing 15 cycles of loading. When the  $MSF$  are plotted versus the number of cycles, as shown in Fig. 14, Seed and Idriss (1982) noted that the factor of safety against liquefaction ( $FS_L$ ) for a soil that liquefied in 10 cycles relative to a total of 15 cycles could be given by the ratio of  $MSF$ s using the equation

$$FS_L = MSF_{15}/MSF_{10} = 1/1.13 = 0.88 \quad (1)$$

Likewise, in our case, the equation can be generalized

$$FS_L = MSF_8/MSF_{\text{cycles to liquefaction}} \quad (2)$$

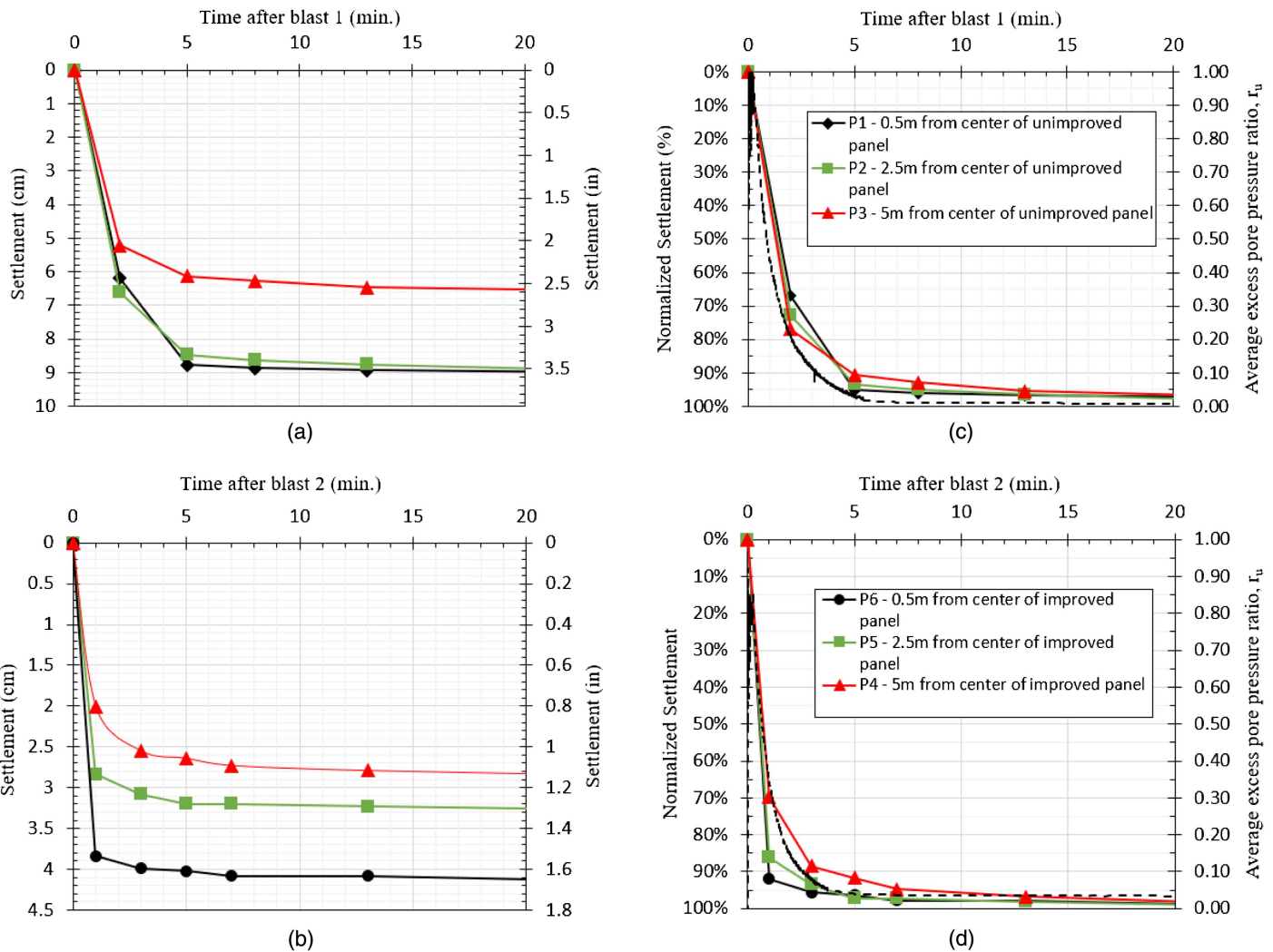


**Fig. 13.** Measured ground settlement with time for (a) NP for Blast 1; and (b) IP for Blast 2 along with the settlement normalized by the maximum settlement for the (c) NP for Blast 1; and (d) IP for Blast 2.

because liquefaction generation was dominated by the detonation of the first eight large charges. The blasting sequence was designed such that the larger 2.0 kg charges, triggered from the 6.5-m depth, would generate the majority of the simulated earthquake energy,

while the smaller 0.5 kg charges at the 3.5-m depth would simply maintain excess pore pressures long enough to observe behavior clearly.

Using Eq. (2), an estimate for the  $FS_L$  was obtained at the depths of each PPT. The PPT data showed that  $r_u$  values reached about 1.0 by the fifth blast, or cycle of loading, at the 4-, 5-, 6-, and 8-m depths corresponding to an  $FS_L$  of 0.9. At depths of 7 and 9 m, this did not occur until the eighth cycle of loading, corresponding to an  $FS_L$  of 1.0. Three  $MSF$  equations were used with Eq. (2) and produced comparable  $FS_L$  for the cycle ratios involved (Seed and Idriss 1982; Idriss and Boulanger 2008; Kayen et al. 2013).

Knowing  $FS_L$ , volumetric strain versus depth could then be computed using the CPT-based equations developed by Zhang et al. (2002) for  $FS_L = 0.9$  and 1.0, respectively

$$\text{For } FS_L = 0.9, \quad \varepsilon_v = 102(q_{c1N})_{cs}^{-0.82} \quad \text{for } 33 \leq (q_{c1N})_{cs} \leq 60 \quad (3)$$

$$\text{For } FS_L = 0.9, \quad \varepsilon_v = 1430(q_{c1N})_{cs}^{-1.48} \quad \text{for } 60 \leq (q_{c1N})_{cs} \leq 200 \quad (4)$$

$$\text{For } FS_L = 1.0, \quad \varepsilon_v = 64(q_{c1N})_{cs}^{-0.93} \quad \text{for } 33 \leq (q_{c1N})_{cs} \leq 60 \quad (5)$$

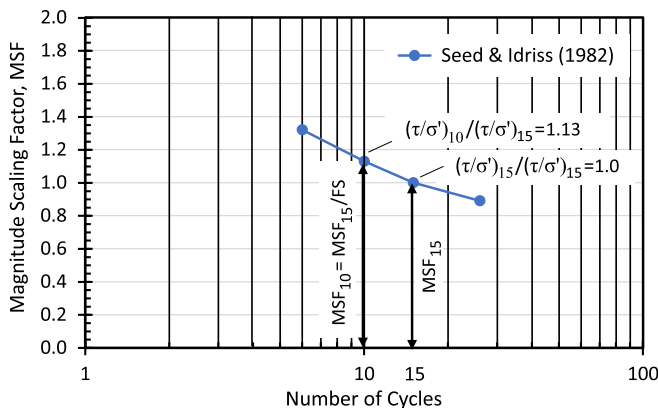


**Fig. 14.** Relationship between magnitude scaling factor (MSF) versus the number of cycles to liquefaction and factor of safety against liquefaction. (Data from Seed and Idriss 1982.)

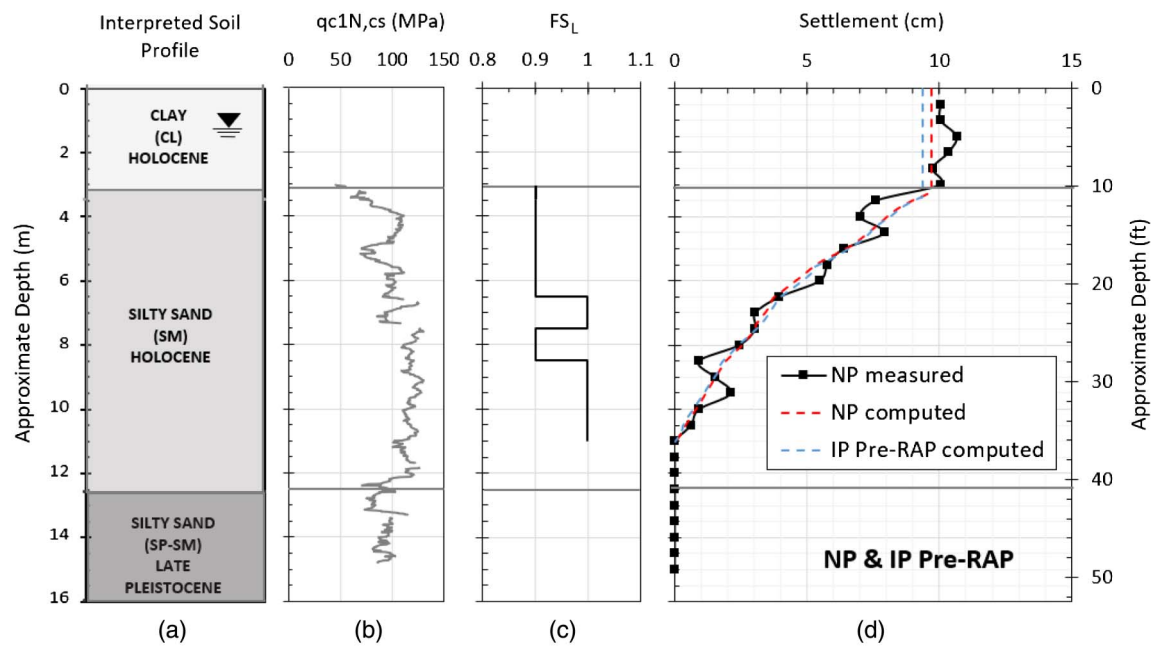


**Fig. 15.** (a) Simplified interpreted soil profile; (b) normalized pre-RAP CPT tip resistance with clean sand correction applied; (c) factor of safety against liquefaction  $FS_L$ ; and (d) comparison of measured and computed settlement versus depth curves in the NP and IP (pre-RAP) using the Zhang et al. (2002) volumetric strain equations based on CPT resistance.

Settlement is simply the volumetric strain multiplied by the vertical layer thickness.

Settlement versus depth plots were thus computed for the CPTu data at the NP area using the volumetric strain equations [Eqs. (3)–(5)] based on  $FS_L$  values shown in Fig. 15(c). Fig. 15(d) shows the computed settlement relative to the measured settlement along with the soil profile and normalized cone tip resistance in Figs. 15(a and b), respectively. The computed settlement is in excellent agreement with the measured settlement versus depth curve with an error of only 4% at the surface, as shown in Fig. 15(d). Fig. 15(d) also shows the computed settlement versus depth curves for the preimprovement IP using the same  $FS_L$  with depth. These estimates are within 3% of each other because there are only minor variations (1%–2%) in the respective  $q_{c1N,cs}$  profiles.

This very good agreement with the measured settlement profile is somewhat surprising considering that postearthquake field studies have found significant differences between measured and computed ground settlement in Christchurch, New Zealand (Geyin and Maurer 2019), and Urayasu, Japan (Katsumata and Tokimatsu 2012). However, there are several factors that could explain this discrepancy. First, postearthquake investigations often rely on SPT or CPT soundings made after the earthquake. After liquefaction, some layers will likely become denser while other layers will become looser (Whitman 1985; Seed 1987). In addition, after liquefaction, the soil microstructure produced by aging will be destroyed and may take many years to redevelop (Andrus et al. 2009). These factors will lead to inaccurate settlement predictions from postearthquake penetration testing. In contrast, the CPT soundings at the Bondeno site were all made before blast-induced liquefaction, avoiding all these problems.

Second, for typical field-case histories, the  $FS_L$  and the thickness of the liquefiable layer must be estimated using a triggering method based on CPT or SPT tests. Errors in these two factors compound the error in estimating settlement. In contrast, at this site, excess pore pressure and settlement were measured versus depths so that the  $FS_L$  and thickness of the liquefied layer were well

defined. Third, there is considerable uncertainty about the effect of fines content on liquefaction resistance, particularly with CPT-based triggering methods. This leads to variability in the predicted liquefaction thickness, the  $FS_L$ , and the resulting computed settlement. By contrast, fines content produced little uncertainty at this site because excess pore pressures were directly measured.

Finally, Cubrinovski et al. (2019) found that there was no difference in the average CPT penetration resistance in the critical liquefaction layers for sites that did and did not manifest liquefaction during the Christchurch earthquake sequence from 2010 to 2011. They attributed the difference in performance to the system response of the profile. Of course, the failure of the CPT to account for system response leads to errors in predicting the resulting settlement. It should be noted that the errors in settlement predictions reported by Geyin and Maurer (2019) were based on case history data from Christchurch. In contrast, at this site, there were no system response issues to complicate settlement calculations, which increases the potential for accurate assessment.

### Computed Settlement of the IP based on Improved CPT Tip Resistance after RAP Installation

The liquefaction-induced settlement following RAP installation was also computed in the IP using the Zhang et al. (2002) volumetric strain equations based on the postinstallation  $q_{c1N,cs}$  profile. Because the average measured peak residual  $r_u$  following the blast in the IP was approximately 0.8, the  $FS_L$  was greater than 1.0. In this case, the  $FS_L$  was computed using a correlation with the measured  $r_u$  proposed by Tokimatsu and Yoshimi (1983) and confirmed by Ishihara (1985), as shown in Fig. 16. This approach was employed by the US Army Corps of Engineers for seismic evaluation of earth dams (Marcuson et al. 1990).

The  $FS_L$  was estimated for each meter of depth between 3 and 9 m according to the  $r_u$  measured by the nearest pore pressure transducer. To evaluate the sensitivity of  $FS_L$  on the settlement, upper- and lower-bound values of  $FS_L$  were also estimated using

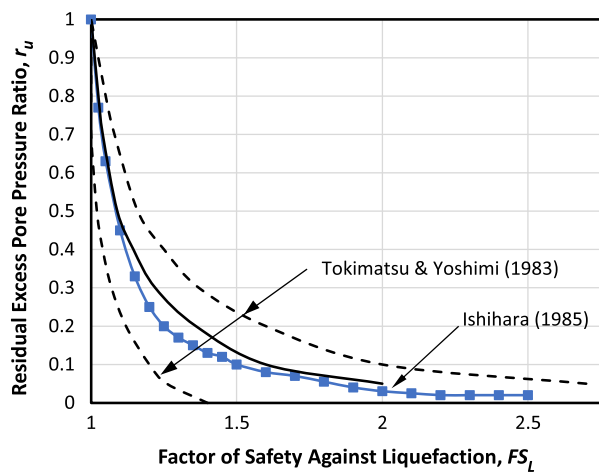


**Fig. 16.** Relationship between the factor of safety against liquefaction ( $FS_L$ ) and residual excess pore pressure ratio ( $r_u$ ). (Data from Tokimatsu and Yoshimi 1983; Ishihara 1985.)

the Tokimatsu and Yoshimi (1983) correlation, as shown in Fig. 17(b). The  $FS_L$  varies between 1 and 1.06 for the test blast in the IP. The higher  $FS_L$  in the IP in comparison with the NP ( $FS_L \approx 0.9$ –1.0) is thought by the authors to be attributable to both the increased relative density and increased lateral earth pressure of the improved soil. The liquefaction-induced volumetric strain for the varying  $FS_L$  at each depth was then interpolated between the curves provided by Zhang et al. (2002) for  $FS_L$  of 1.0 [Eq. (5)] and 1.1 given by

$$\text{For } FS_L = 1.1, \quad \varepsilon_v = 11(q_{c1N})_{cs}^{-0.65} \quad \text{for } 33 \leq (q_{c1N})_{cs} \leq 200 \quad (6)$$

The Zhang et al. (2002) method was also used to compute the volumetric strain for the zone beneath the limits of the RAP

treatment (9.5–11 m) using the same approach as for the untreated soil described previously.

The computed settlement versus depth curve is compared with the measured curve in Fig. 17(c), and it is clear that the range in  $FS_L$  had very little effect on the computed settlement. The computed curve estimates a settlement of about 5 cm in the RAP treatment zone in comparison to the measured settlement of about 2 cm, which represents an overestimation of about 150%. This overestimation suggests that some other mechanism may be responsible for the reduction in the settlement that occurred, which will be explored in the next section.

### Computed Settlement of the IP based on Improved CPT Tip Resistance Combined with RAP Axial Stiffness

The predicted settlement of the IP using the Zhang (2002) volumetric strain equations in the previous section neglects the axial stiffness of the RAPs during liquefaction. Axial stiffness was recognized by Martin et al. (2004) to be an important part of settlement reduction for a site treated with jet grouted columns during the  $M_w$  7.6 Kocaeli earthquake in Turkey. Moreover, Adalier et al. (2003) reported that stone columns in a silt matrix reduced foundation settlement by 50% owing to the increased average soil stiffness despite liquefaction in the silt matrix. Finally, Lawton and Fox (1994) recommend a composite modulus approach to consider the axial stiffness of the RAP in computing soil settlement after RAP treatment.

Fig. 18 shows a schematic drawing of the response of the treated ground as a result of postblast liquefaction settlement. Fig. 8 shows that the blasting increased the pore water pressure in the IP to  $r_u$  values ranging between 0.74 and 0.97, with a consequent reduction in vertical effective stress. The postblast dissipation of these pore water pressures reinstates the vertical effective stress resulting in a settlement in the soil that may be predicted using the Zhang (2002) equations as in shown Fig. 17. Postliquefaction settlements result in downward movement of the soil relative to the dense nonliquefiable RAPs resulting in stress transfer from the soil to the RAPs, which decreases the value of reinstated vertical effective stress in the soil

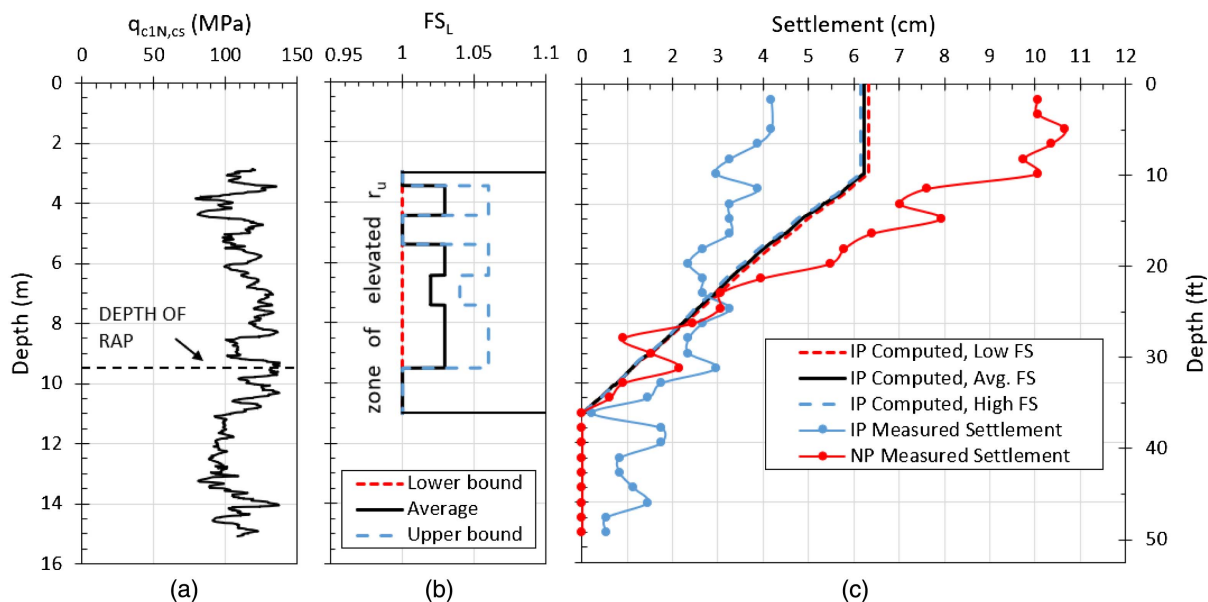


**Fig. 17.** (a) Normalized CPT tip resistance with clean sand correction  $(q_{c1N})_{cs}$  in the post-RAP IP; (b) upper-bound, average, and lower-bound values of  $FS_L$  with depth using the Tokimatsu and Yoshimi (1983)  $FS_L$  versus  $r_u$  correlation; and (c) observed settlement in the NP and the IP alongside the computed settlement in IP considering the effects of increased cone tip resistance using volumetric strain equations from Zhang et al. (2002).

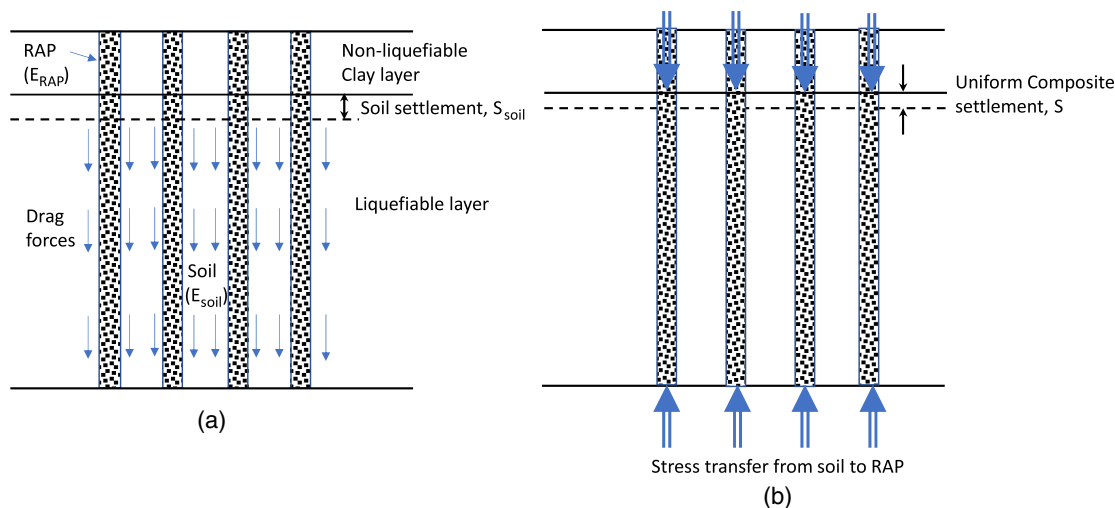


**Fig. 18.** Schematic drawing illustrating (a) settlement of soil,  $S_{soil}$ , with the constrained modulus ( $M_{soil}$ ) transferring load to stiffer nonliquefied RAPs with a higher modulus ( $M_{RAP}$ ) to produce (b) reduced uniform composite settlement,  $S$ , with an increased load in the RAPs.

and increases the effective vertical stress in the RAPs. The amount of stress transfer depends on the relative stiffness of the materials and the boundary conditions at the top and bottom of the system. For conditions in which the top and bottom boundary conditions are rigid, the settlement ( $S$ ) is uniform and may be estimated using a simple expression

$$S = \frac{qIH}{M_{composite}} \quad (7)$$

where  $q$  = applied change in pressure;  $I$  = influence factor (unity);  $H$  = layer thickness; and  $M_{composite}$  = composite constrained modulus value (Han 2015). Values for  $q$  may be estimated as the reinstated vertical effective stress value computed as the product of the initial vertical effective stress and the layer  $r_u$  value. The composite constrained modulus value may be estimated from the average constrained modulus value for the postblast response of the soil ( $M_{soil}$ ), the postblast constrained modulus of the RAP ( $M_{RAP}$ ), and the area replacement ratio of the RAP ( $R_a$ ) with the equation

$$M_{composite} = M_{soil}(1 - R_a) + M_{RAP}R_a \quad (8)$$

The postblast constrained modulus value for the soil may be back-calculated using the equation

$$M_{soil} = \frac{qIH}{S_{soil}} \quad (9)$$

where  $q$  = reinstated vertical effective stress value in the soil layer computed as the product of the initial vertical effective stress and the average layer  $r_u$  value;  $I$  = unity; and  $S_{soil}$  = settlement of the soil between the RAPs after treatment computed using the Zhang et al. (2002) approach, equal to 5 cm, as described in the previous section and shown in Fig. 17(c).

The postblast constrained modulus ( $M_{RAP}$ ) for the RAPs may be computed using the standard equation to convert from the elastic modulus for the RAP and a reduction factor for reduced confining pressure as given by the equation

$$M_{RAP} = \frac{E_{RAP}(1 - \nu)(R_\sigma)}{(1 + \nu)(1 - 2\nu)} \quad (10)$$

where Poisson's ratio ( $\nu$ ) = 0.3; and the elastic modulus value for the RAP ( $E_{RAP}$ ) is taken as 192 MPa (4,000 ksf) based on the average elastic modulus from a database of full-scale field load tests on RAPs (Wissmann et al. 2001). For a large project in practice, a load test could be performed on a pier to determine the elastic modulus directly. When excess pore pressures develop in the soil surrounding a RAP, the effective confining pressure decreases, reducing the modulus as a function of the square root of the decreased pressure (Duncan and Chang 1970). The reduction in the modulus can then be estimated using a reduction factor ( $R_\sigma$ ) given by the equation

$$R_\sigma = \left[ 1 - \frac{(r_u)_{avg}}{2} \right]^{0.5} \quad (11)$$

where  $(r_u)_{avg}$  = average excess pore pressure ratio in the treated zone after blasting (or an earthquake); and  $(r_u)_{avg}/2$  = average excess pressure during reconsolidation to static water pressure. Using Eqs. (10) and (11) with a Poisson's ratio of 0.3, the postblast  $M_{RAP}$  for  $(r_u)_{avg}$  of 0.86, in this case, would be 195 MPa. Based on Eq. (8), with an area replacement ratio of only 5%, the piers account for 53% of the  $M_{composite}$  and increase the  $M_{composite}$  by a factor of 2.1 relative to  $M_{soil}$ .

Applying Eq. (7) yields a settlement of 1.86 cm in the treated zone from 3 to 9.5 m relative to the measured value of about 2.0 cm. Applying Eq. (7) incrementally produces the computed settlement versus depth profile in Fig. 19, which is in good agreement with the measured curve. Variations of  $\pm 25\%$  in the value of  $M_{RAP}$  lead to variations in the computed settlement of about  $\pm 15\%$ , as shown in Fig. 19. The applicability of the composite settlement approach is also corroborated by the noted uniformity of the surficial settlements postulated in Fig. 18(b) and observed both visually and in the TLS plot shown in Fig. 11.

It seems reasonable to expect that other methods for installing dense granular columns (DGCs) may also be able to reduce liquefaction-induced settlement by similar mechanisms to those presented for the RAP group in this study. However, similar field testing would be desirable to confirm this performance, and field test data defining DGC stiffness would be necessary.

Observed settlement of about 1 cm below 11 m in the IP is likely a result of the stress transfer into the RAP columns, as illustrated in Fig. 18(b). A number of approaches could be used to

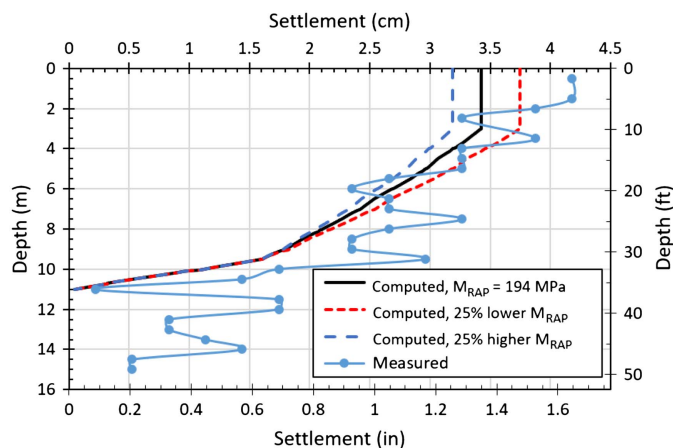


**Fig. 19.** Comparison of measured settlement versus depth with settlement curves computed using a composite modulus approach with best-estimate  $M_{RAP}$  and  $\pm 25\%$  higher and lower  $M_{RAP}$  values in the IP.

estimate this settlement, but the test results do not provide sufficient information to confirm the validity of any specific mechanism.

## Summary and Conclusions

Full-scale blast-induced liquefaction tests were carried out in Bondeno, Italy, to evaluate the effectiveness of RAP treatment in mitigating liquefaction hazards in Holocene silty sands (fines content  $\approx 15\%$ – $45\%$ ). Blast tests were performed on natural and improved panels at a test site where silty sands liquefied and produced numerous sand boils during the 2012  $M_w$  6.1 Emilia Romagna earthquake. The RAPs consisted of a 0.5 m diameter dense gravel columns installed to a target depth of 9.5 m in a  $4 \times 4$  arrangement at a 2-m center-to-center spacing with a replacement ratio of 5%. The consistent nature of the soil profile between the natural and improved panels provided an excellent window for observing the mitigating effects of RAP improvement related to liquefaction. Pore pressure transducers and settlement monitoring provided detailed information about the performance of the two panels.

Based on the field testing and subsequent data analysis, the following conclusions can be drawn:

- Blasting produced liquefaction and induced settlement of 8.5 cm in the natural panel (NP) from 3 to 9.5 m. Several large sand boils developed following blasting. The computed settlement versus depth curve using the CPT-based volumetric strain equations proposed by Zhang et al. (2002) produced a very good agreement with the measured curve.
- RAP installation densified the silty sand, increasing  $q_t$  by about 30%. Post-RAP  $K_0$  values increased about 30% between the 4- and 7-m depth and 100% between the 7- and 9-m depth in comparison to the natural soil conditions.
- Installation of the RAP group decreased settlement after blasting to about 2 cm within the treated zone from 3 to 9.5 m, relative to 8.5 cm in the untreated area (76% improvement), despite the fact that  $r_u$  values of 74%–100% still developed within the soil between the RAPs. No sand boils erupted within the treated area in the improved panel (IP).
- The reduction in excess pore pressure-induced settlement in the IP could not be reasonably explained by the densification measured by the posttreatment CPT soundings. The Zhang et al. (2002) CPT-based volumetric strain equations overestimated

the measured settlement by 150% when considering densification effects alone.

- The measured settlement versus depth profile within the RAP treatment zone was reasonably well computed, assuming that the RAPs stiffen the surrounding sand and resist liquefaction-induced compression as a composite during pore pressure dissipation.

## Data Availability Statement

Some or all data, models, or code that support the findings of this study are available from the corresponding author upon reasonable request. These data include in situ test results, excess pore pressure response, settlement versus depth curves, and settlement versus time curves.

## Acknowledgments

Financial support for this study was primarily provided by the Geopier Foundation Company along with RAP-licensed contractor, Releo s.r.l. (Ferrara, Italy), who provided the installation of the rammed aggregate piers free of charge. In addition, funding for Mr. Anderson was provided by an REU supplement to Grant No. CMMI-1663288 from the National Science Foundation. This funding is gratefully acknowledged. However, the opinions, conclusions, and recommendations in this paper do not necessarily represent those of the sponsors. From the Italian side, additional funding was provided by the INGV-FIRB Abruzzo project (*Indagini ad alta risoluzione per la stimadella pericolosità e del rischio sismico nelle aree colpite dal terremoto del 6 Aprile 2009*), by the INGV-Abruzzo Region project (*Indagini di geologia, sismologia e geodesia per la mitigazione del rischio sismico*, L.R. n. 37/2016), and by the CIRI Edilizia e Costruzioni, University of Bologna, Italy (TIRISICO PROJECT *Tecnologie Innovative per la riduzione del rischio sismico delle Costruzioni*, Project No. PG/2015/ 737636, POR-FESR 2014-2020). We also express our appreciation to the Bondeno Municipality and to the Emilia-Romagna Region, who provided all the necessary support to realize the research in collaboration with the other local authorities (Ferrara Prefecture, Ferrara Province, Local Civil Protection, Police).

## References

- Adalier, K., and A. Elgamil. 2004. "Mitigation of liquefaction and associated ground deformations by stone columns." *J. Eng. Geol.* 72 (3–4): 275–291. <https://doi.org/10.1016/j.enggeo.2003.11.001>.
- Adalier, K., A. Elgamil, J. Meneses, and J. I. Baez. 2003. "Stone columns as liquefaction countermeasure in non-plastic silty soils." *Soil Dyn. Earthquake Eng.* 23 (7): 571–584. [https://doi.org/10.1016/S0267-7261\(03\)00070-8](https://doi.org/10.1016/S0267-7261(03)00070-8).
- Allen, M. G., R. Jones, and F. B. Gularte. 1995. "Bottom-feed stone columns, wet-replacement construction method Mormon Island Auxiliary Dam modifications." In *Soil Improvement for Earthquake Hazard Mitigation*, Geotechnical Special Publication 49, 82–93. Reston, VA: ASCE.
- Amoroso, S., et al. 2020. "Blast-induced liquefaction in silty sands for full-scale testing of ground improvement methods: Insights from a multi-disciplinary study." *Eng. Geol.* 265 (Feb): 105437. <https://doi.org/10.1016/j.enggeo.2019.105437>.
- Amoroso, S., K. M. Rollins, P. Monaco, M. Holtrigter, and A. Thorp. 2018. "Monitoring ground improvement using the seismic dilatometer in Christchurch, New Zealand." *Geotech. Test. J.* 41 (5): 20170376. <https://doi.org/10.1520/GTJ20170376>.

- Andrus, R. D., H. Hayati, and N. P. Mohanan. 2009. "Correcting liquefaction resistance for aged sands using measured to estimated velocity ratio." *J. Geotech. Geoenviron. Eng.* 135 (6): 735–744. [https://doi.org/10.1061/\(ASCE\)GT.1943-5606.0000025](https://doi.org/10.1061/(ASCE)GT.1943-5606.0000025).
- Ashford, S. A., K. M. Rollins, S. C. Bradford, T. J. Weaver, and J. I. Baez. 2000. "Liquefaction mitigation using stone columns around deep foundations: Full scale test results." *Transp. Res. Rec.* 1736 (1): 110–118. <https://doi.org/10.3141/1736-14>.
- Baez, J. I. 1995. "A design model for the reduction of soil liquefaction by vibrostone columns." Ph.D. thesis, Dept. of Civil Engineering, Univ. of Southern California.
- Baldi, G., R. Bellotti, V. Ghionna, M. Jamiolkowski, S. Marchetti, and E. Pasqualini. 1986. "Flat dilatometer tests in calibration chambers." In *Proc., Specialty Conf. on Use of In Situ Tests in Geotechnical Engineering*, 431–446. Reston, VA: ASCE.
- Boulanger, R. W., and I. M. Idriss. 2016. "CPT-based liquefaction triggering procedure." *J. Geotech. Geoenviron. Eng.* 142 (2): 1413–1426. [https://doi.org/10.1061/\(ASCE\)GT.1943-5606.0001388](https://doi.org/10.1061/(ASCE)GT.1943-5606.0001388).
- Bray, J. D., and R. B. Sancio. 2006. "Assessment of the liquefaction susceptibility of fine-grained soils." *J. Geotech. Geoenviron. Eng.* 132 (9): 1165–1177. [https://doi.org/10.1061/\(ASCE\)1090-0241\(2006\)132:9\(1165\)](https://doi.org/10.1061/(ASCE)1090-0241(2006)132:9(1165)).
- Castro, G. 1969. "Liquefaction of sands." Ph.D. dissertation, Div. of Engineering and Applied Physics, Harvard Univ.
- CEN (European Committee for Standardization). 2004. *Eurocode 8—Design of structures for earthquake resistance. Part 1: General rules, seismic actions and rules for buildings*. EN 1998-1:2004. Brussels, Belgium: European Committee for Standardization.
- Cubrinovski, M., A. Rhodes, N. Ntritsos, and S. Van Ballegooy. 2019. "System response of liquefiable deposits." *J. Soil Dyn. Earthquake Eng.* 124 (Sep): 212–229. <https://doi.org/10.1016/j.soildyn.2018.05.013>.
- D'Appolonia, E. 1954. "Loose sands—Their compaction by vibroflotation." In *Proc., Symp. on ASTM Int.*, 138–162. West Conshohocken, PA: ASTM.
- Demir, S., P. Özener, M. Kirkit, and P. Özener. 2017. "Experimental and numerical investigations of behavior of rammed aggregate piers." *Geotech. Test. J.* 40 (3): 411–425. <https://doi.org/10.1520/GTJ20150195>.
- Duncan, J. M., and C.-Y. Chang. 1970. "Nonlinear analysis of stress and strain in soils." *J. Soil Mech. Found. Div.* 96 (5): 1629–1653.
- Emergo Working Group. 2013. "Liquefaction phenomena associated with the Emilia earthquake sequence of May-June 2012 (Northern Italy)." *Nat. Hazards Earth Syst. Sci.* 13 (4): 935–947. <https://doi.org/10.5194/nhess-13-935-2013>.
- Gallagher, P., C. T. Conlee, and K. M. Rollins. 2007. "Full-scale field testing of colloidal silica grouting for mitigation of liquefaction risk." *J. Geotech. Geoenviron. Eng.* 133 (2): 186–196. [https://doi.org/10.1061/\(ASCE\)1090-0241\(2007\)133:2\(186\)](https://doi.org/10.1061/(ASCE)1090-0241(2007)133:2(186)).
- Geopier Foundation Company. 2019. *Rammed aggregate pier construction and quality control procedures for the Impact system*. Davidson, North Carolina: Geopier Foundation Company.
- Geyin, M., and B. W. Maurer. 2019. "An analysis of liquefaction-induced free-field ground settlement using 1,000+ case-histories: Observations vs. state-of-practice predictions." In *Gecongress 2019: Earthquake engineering and soil*, 489–498. Reston, VA: ASCE.
- Gianella, T. N., and A. W. Stuedlein. 2017. "Performance of driven displacement pile-improved ground in controlled blasting field tests." *J. Geotech. Geoenviron. Eng.* 143 (9): 04017047. [https://doi.org/10.1061/\(ASCE\)GT.1943-5606.0001731](https://doi.org/10.1061/(ASCE)GT.1943-5606.0001731).
- Goughnour, R. R., and J. M. Pestana. 1998. "Mechanical behavior of stone columns under seismic loading." In *Proc., 2nd Int. Conf. on Ground Improvement Techniques*. Singapore: Ci-Premier.
- Green, R. A., C. G. Olgun, and K. J. Wissmann. 2008. "Shear stress redistribution as a mechanism to mitigate the risk of liquefaction." In *Geotechnical earthquake engineering and soil dynamics IV*. Reston, VA: ASCE.
- Han, J. 2015. *Principles and practices of ground improvement*. Hoboken, NJ: Wiley.
- Harada, K., R. P. Orense, K. Ishihara, and J. Mukai. 2010. "Lateral stress effects on liquefaction resistance correlations." *Bull. New Zealand Soc. Earthquake Eng.* 43 (1): 13–23. <https://doi.org/10.5459/bnzsee.43.1.13-23>.
- Idriss, I. M., and R. W. Boulanger. 2008. *Soil liquefaction during earthquakes*. Monograph MNO-12. Oakland, CA: Earthquake Engineering Research Institute.
- Ishihara, K. 1985. "Stability of natural deposits during earthquakes." In *Proc., Int. Conf. on Soil Mechanics and Foundation Engineering*, 321–376. Boca Raton, FL: CRC Press.
- Ishihara, K., and M. Yoshimine. 1992. "Evaluation of settlements in sand deposits following liquefaction during earthquakes." *Soils Found.* 32 (1): 173–188. <https://doi.org/10.3208/sandf1972.32.173>.
- Jamiolkowski, M., D. C. F. Lo Presti, and M. Manassero. 2003. "Evaluation of relative density and shear strength of sands from cone penetration test and flat dilatometer test." In *Soil behaviour and soft ground construction*, 201–238. Reston, VA: ASCE.
- Katsumata, K., and K. Tokimatsu. 2012. "Relationship between seismic characteristics and soil liquefaction of Urayasu city induced by the 2011 Great East Japan Earthquake." In *Proc., 9th Intl. Conf. on Urban Earthquake Engineering*, 601–606. Tokyo: Tokyo Institute of Technology.
- Kayen, R., R. E. S. Moss, E. M. Thompson, R. B. Seed, K. O. Cetin, A. Der Kiureghian, Y. Tanaka, and K. Tokimatsu. 2013. "Shear-wave velocity-based probabilistic and deterministic assessment of seismic soil liquefaction potential." *J. Geotech. Eng.* 139 (3): 407–419. [https://doi.org/10.1061/\(ASCE\)GT.1943-5606.0000743](https://doi.org/10.1061/(ASCE)GT.1943-5606.0000743).
- Lawton, E. C., and N. S. Fox. 1994. "Settlement of structures supported on marginal or inadequate soils stiffened with short aggregate piers." In *Proc., Settlement '94 Vertical and Horizontal Deformations of Foundations and Embankments*, 962–974. Reston, VA: ASCE.
- Lawton, E. C., and S. M. Merry. 2000. *Performance of Geopier reinforced soil foundations during simulated seismic tests on I-15 bridge bents*, 3–11. Washington, DC: Transportation Research Board.
- Luehring, R., N. Snortland, M. Stevens, and L. Mejia. 2001. *Liquefaction mitigation of a silty dam foundation using vibro-stone columns and drainage wicks: A case history at Salmon Lake Dam*, 1–15. Washington, DC: US Bureau of Reclamation.
- Majchrzak, M., T. Farrell, and B. Metcalfe. 2009. "Innovative soil reinforcement method to control static and seismic settlements." In *Proc., Int. Foundation Congress and Equipment Expo*. Reston, VA: ASCE.
- Marchetti, D., P. Monaco, S. Amoroso, and L. Minarelli. 2019. "In situ tests by Medusa DMT." In *Proc., 17th European Conf. on Soil Mechanics and Geotechnical Engineering ECSMGE-2019*. Reykjavik, Iceland: Icelandic Geotechnical Society.
- Marchetti, S. 1980. "In situ tests by flat dilatometer." *J. Geotech. Eng. Div.* 106 (3): 299–321. <https://doi.org/10.1061/AJGEB6.0000934>.
- Marchetti, S., P. Monaco, G. Totani, and D. Marchetti. 2008. *In situ tests by seismic dilatometer (SDMT)*. Reston, VA: ASCE.
- Marcuson, W. F., M. E. Hynes, and A. G. Franklin. 1990. "Evaluation and use of residual strength in seismic safety analysis of embankments." *Earthquake Spectra* 6 (3): 529–572. <https://doi.org/10.1193/1.1585586>.
- Martin, J. R., C. G. Olgun, J. K. Mitchell, and H. T. Durgunoglu. 2004. "High-modulus columns for liquefaction mitigation." *J. Geotech. Geoenviron. Eng.* 130 (6): 561–571. [https://doi.org/10.1061/\(ASCE\)1090-0241\(2004\)130:6\(561\)](https://doi.org/10.1061/(ASCE)1090-0241(2004)130:6(561)).
- Maurer, B. W., R. A. Green, S. van Ballegooy, and L. Wotherspoon. 2019. "Development of region-specific soil behavior type index correlations for evaluating liquefaction hazard in Christchurch, New Zealand." *Soil Dyn. Earthquake Eng.* 117 (Feb): 96–105. <https://doi.org/10.1016/j.soildyn.2018.04.059>.
- Meletti, C., F. Galadini, G. Valensise, M. Stucchi, R. Basili, S. Barba, G. Vannucci, and E. Boschi. 2008. "A seismic source zone model for the seismic hazard assessment of the Italian territory." *Tectonophysics* 450 (1–4): 85–108. <https://doi.org/10.1016/j.tecto.2008.01.003>.
- Mitchell, J. 1981. "Soil improvement—State-of-the-art report." In *Proc., 10th Int. Conf. on Soil Mechanics and Foundation Engineering*, 509–565. Rotterdam, Netherlands: A.A. Balkema.
- Namikawa, T., J. Koseki, and Y. Suzuki. 2017. "Finite element analysis of lattice-shaped round improvement by cement-mixing for liquefaction

- mitigation." *Soils Found. Jpn. Geotech. Soc.* 47 (1): 559–576. Tokyo: Japanese Geotechnical Society.
- Olgun, C. G. 2003. "Performance of improved ground and reinforced soil structures during earthquakes—Case studies and numerical analyses." Ph.D. thesis, Dept. of Civil and Environmental Engineering, Virginia Tech.
- Priebe, H. J. 1995. "The design of vibro replacement." *Ground Eng.* 28 (10): 31–46. [https://doi.org/10.1016/0148-9062\(96\)80092-1](https://doi.org/10.1016/0148-9062(96)80092-1).
- Priebe, H. J. 1998. "Vibro replacement to prevent earthquake induced liquefaction." *Ground Eng.* 31 (9): 30–33.
- Rayamajhi, D., R. W. Boulanger, S. A. Ashford, and A. Elgamal. 2015. "Dense granular columns in liquefiable ground. II: Effects on deformations." *J. Geotech. Geoenviron. Eng.* 142 (7): 04016024. [https://doi.org/10.1061/\(ASCE\)GT.1943-5606.0001475](https://doi.org/10.1061/(ASCE)GT.1943-5606.0001475).
- Regione Emilia-Romagna. 1998. *Riserve idriche sotterranee della Regione Emilia-Romagna*. Bologna, Italy: Emilia-Romagna Region.
- Robertson, P. K., and C. E. Wride. 1998. "Evaluating cyclic liquefaction potential using the cone penetration test." *Can. Geotech.* 35 (3): 442–459. <https://doi.org/10.1139/t98-017>.
- Rollins, K. M., T. M. Gerber, J. D. Lane, and S. A. Ashford. 2005. "Lateral resistance of a full-scale pile group in liquefied sand." *J. Geotech. Geoenviron. Eng.* 131 (1): 115–125. [https://doi.org/10.1061/\(ASCE\)1090-0241\(2005\)131:1\(115\)](https://doi.org/10.1061/(ASCE)1090-0241(2005)131:1(115)).
- Rollins, K. M., R. R. Goughnour, J. K. S. Anderson, and A. McCain. 2004. "Liquefaction hazard mitigation using vertical composite drains." In *Proc., 13th World Conf. on Earthquake Engineering*. Oakland, CA: EERI.
- Rollins, K. M., M. Quimby, S. R. Johnson, and B. Price. 2009. "Effectiveness of stone columns for liquefaction mitigation of silty sands with and without wick drains." In *Proc., U.S.-China Workshop on Ground Improvement*. Reston, VA: ASCE.
- Rollins, K. M., A. Wright, D. Sjoblom, N. White, and C. Lange. 2012. "Evaluation of liquefaction mitigation with stone columns in interbedded silts and sands." In *Proc., 4th Int. Conf. on Geotechnical and Geophysical Site Characterization*, 1469–1475. London: Taylor and Francis Group.
- Saftner, D. A., J. Zheng, R. A. Green, R. Hryciw, and K. Wissmann. 2018. *Rammed aggregate pier installation effect on soil properties*, 63–73. London: ICE Publishing.
- Saito, A. 1977. "Characteristics of penetration resistance of a reclaimed sandy deposit and their changes through vibratory compaction." *Soils Found.* 17 (4): 31–43. [https://doi.org/10.3208/sandf1972.17.4\\_31](https://doi.org/10.3208/sandf1972.17.4_31).
- Seed, H. B. 1987. "Design problems in soil liquefaction." *J. Geotech. Eng.* 113 (8): 827–845. [https://doi.org/10.1061/\(ASCE\)0733-9410\(1987\)113:8\(827\)](https://doi.org/10.1061/(ASCE)0733-9410(1987)113:8(827)).
- Seed, H. B., and I. M. Idriss. 1982. "Ground motions and soil liquefaction during earthquakes." In *Monograph series*, 130. Oakland, CA: EERI.
- Smith, M., and K. Wissmann. 2018. "Ground improvement reinforcement mechanisms determined for the Mw 7.8 Muisne, Ecuador, Earthquake." *Geotech. Earthquake Eng. Soil Dyn.* 5 (Jun): 10–13. <https://doi.org/10.1061/9780784481455.028>.
- Stucchi, M., C. Meletti, V. Montaldo, H. Crowley, G. M. Calvi, and E. Boschi. 2011. "Seismic hazard assessment (2003–2009) for the Italian building code." *Bull. Seismol. Soc. Am.* 101 (4): 1885–1911. <https://doi.org/10.1785/0120100130>.
- Studer, J., and L. Kok. 1980. "Blast-induced excess porewater pressure and liquefaction; Experience and application." In *Proc., Int. Symp. on Soils Under Cyclic and Transient Loading*, 581–593. Rotterdam, Netherlands: A.A. Balkema.
- Tokimatsu, K., and Y. Yoshimi. 1983. "Empirical correlation of soil liquefaction based on SPT N-value and fines content." *Soils Found.* 23 (4): 56–74. [https://doi.org/10.3208/sandf1972.23.4\\_56](https://doi.org/10.3208/sandf1972.23.4_56).
- van Ballegooy, S., P. Malan, V. Lacrosse, M. E. Jacka, M. Cubrinovski, J. D. Bray, T. D. O'Rourke, S. A. Crawford, and H. Cowan. 2014. "Assessment of liquefaction-induced land damage for residential Christchurch." *Earthquake Spectra* 30 (1): 31–55. <https://doi.org/10.1193/031813EQS070M>.
- Vautherin, E., C. Lambert, D. Barry-Macaulay, and M. Smith. 2017. "Performance of rammed aggregate piers as a soil densification method in sandy and silty soils: Experience from the Christchurch rebuild." In *Proc., 3rd Int. Conf. on Performance-based Design in Earthquake Geotechnical Engineering—PBD-III*. London: International Society for Soil Mechanics and Geotechnical Engineering.
- Weaver, T., S. Ashford, and K. M. Rollins. 2004. "Performance and analysis of a laterally loaded pile in stone column improved ground." In *Proc., 13th World Conf. on Earthquake Engineering*, Vancouver, BC, Canada: Canadian Association for Earthquake Engineering.
- Wentz, F. J., S. van Ballegooy, K. M. Rollins, S. A. Ashford, and M. J. Olsen. 2015. "Large scale testing of shallow ground improvements using blast-induced liquefaction." In *Proc., 6th Int. Conf. on Earthquake Geotechnical Engineering—6ICEGE*. London: International Society for Soil Mechanics and Geotechnical Engineering.
- White, D. J., M. T. Suleiman, H. T. Pham, and J. Bigelow. 2002. *Constitutive equations for aggregates used in Geopier® foundation construction*. Ames, IA: Iowa State Univ.
- Whitman, R. V. 1985. "On liquefaction." In *Proc., 11th Int. Conf. on Soil Mechanical and Foundation Engineering*, 1923–1926. Rotterdam, Netherlands: A.A. Balkema.
- Wissmann, K. J., K. Moser, and M. Pando. 2001. "Reducing settlement risks in residual piedmont soils using rammed aggregate pier elements." In *Proc., ASCE Specialty Conf.* Reston, VA: ASCE.
- Wissmann, K. J., S. van Ballegooy, B. C. Metcalfe, J. N. Dismuke, and C. K. Anderson. 2015. "Rammed aggregate pier ground improvement as liquefaction method in sandy and silty soils." In *Proc., 6th Int. Conf. on Earthquake Geotechnical Engineering—6ICEGE*. London: International Society for Soil Mechanics and Geotechnical Engineering.
- Youd, T. L., et al. 2001. "Liquefaction resistance of soils: Summary report from the 1996 NCEER and 1998 NCEER/NSF workshops on evaluation of liquefaction resistance of soils." *J. Geotech. Geoenviron. Eng.* 127 (10): 817–833. [https://doi.org/10.1061/\(ASCE\)1090-0241\(2001\)127:4\(297\)](https://doi.org/10.1061/(ASCE)1090-0241(2001)127:4(297)).
- Zhang, G., P. K. Robertson, and R. W. I. Brachman. 2002. "Estimating liquefaction-induced ground settlements from CPT for level ground." *Can. Geotech. J.* 39 (5): 1168–1180. <https://doi.org/10.1139/t02-047>.